Quaternary Science Reviews 71 (2013) 91–108

Contents lists available at SciVerse ScienceDirect

Quaternary Science Reviews

journal homepage: www.elsevier.com/locate/quascirev

High-resolution paleomagnetic secular variations and relative paleointensity since the Late Pleistocene in southern South America

Agathe Lisé-Pronovost [a,b,*], Guillaume St-Onge [a,b], Claudia Gogorza [c], Torsten Haberzettl [d], Michel Preda [e], Pierre Kliem [f], Pierre Francus [b,g], Bernd Zolitschka [f], The PASADO Science Team [1]

[a] Canada Research Chair in Marine Geology, Institut des sciences de la mer de Rimouski (ISMER), Université du Québec à Rimouski (UQAR), Rimouski, Canada
[b] GEOTOP Research Center, Canada
[c] Instituto de Física Arroyo Seco, Universidad Nacional del Centro de la Provincia de Buenos Aires, Tandil, Argentina
[d] Physical Geography, Friedrich-Schiller-University Jena, Jena, Germany
[e] Département des sciences de la Terre et de l'atmosphère, Université du Québec à Montréal (UQAM), Montréal, Canada
[f] Geomorphology and Polar Research (GEOPOLAR), Institute of Geography, University of Bremen, Bremen, Germany
[g] Institut national de la recherche scientifique, centre Eau, Terre, Environnement (INRS-ETE), Québec, Canada

ARTICLE INFO

Article history:
Received 13 December 2011
Received in revised form
9 May 2012
Accepted 14 May 2012
Available online 14 June 2012

Keywords:
ICDP-project PASADO
Laguna Potrok Aike
Paleomagnetism
Relative paleointensity
Secular variation
Southern Hemisphere

ABSTRACT

Paleomagnetic inclination, declination and relative paleointensity were reconstructed from the sediments of Laguna Potrok Aike in the framework of the International Continental scientific Drilling Program (ICDP) Potrok Aike maar lake Sediment Archive Drilling prOject (PASADO). Here we present the u-channel-based full vector paleomagnetic field reconstruction since 51.2 ka cal BP. The relative paleointensity proxy (RPI) was built by normalising the natural remanent magnetisation with the anhysteretic remanent magnetisation using the average ratio at 4 demagnetisation steps part of the ChRM interval ($NRM/ARM_{10-40\ mT}$). A grain size influence on the RPI was removed using a correction based on the linear relationship between the RPI and the median destructive field of the natural remanent magnetisation (MDF_{NRM}). The new record is compared with other lacustrine and marine records and stacks from the mid- to high-latitudes of the Southern Hemisphere, revealing consistent millennial-scale variability, the identification of the Laschamp and possibly the Mono Lake geomagnetic excursions, and a direction swing possibly associated to the Hilina Pali excursion at 20 ka cal BP. Nonetheless, a global-scale comparison with other high-resolution records located on the opposite side of the Earth and with various dipole field references hint at a different behaviour of the geomagnetic field around southern South America at 46 ka cal BP.

1. Introduction

Geological archives such as marine and lacustrine sediments are the only way to reconstruct the past millennial- to centennial-scale variability of the geomagnetic field beyond historical time; however the uneven distribution of the records on Earth does not allow addressing the possible global nature of its variability. The reason for this geographical bias is that high-resolution paleomagnetic records from the Southern Hemisphere are rare. As a consequence, global stacks are truly derived from a majority of records located in the Northern Hemisphere (e.g., GLOPIS-75, Laj et al., 2004; SINT-200, Guyodo and Valet, 1996) and geomagnetic field models lack calibration data from the Southern Hemisphere in order to better understand the core geodynamics (e.g., Korte et al., 2005; Roberts, 2008; Korte and Constable, 2011). A major limit to the collection of high-resolution records from the Southern Hemisphere is the scarcity of adequately high sedimentation rate basins and their accessibility. In particular, the mid-latitudes of the Southern Hemisphere are dominated by the open ocean realm with its typically low accumulation rates (e.g., Lund et al., 2006a) and south of 48°S, the South American continent is the only land mass beside islands in the Southern Ocean and the ice-covered Antarctica.

* Corresponding author. Canada Research Chair in Marine Geology, Institut des sciences de la mer de Rimouski (ISMER), Université du Québec à Rimouski (UQAR), Rimouski, Canada.
E-mail address: agathe.lisepronovost@uqar.qc.ca (A. Lisé-Pronovost).
[1] http://www.icdp-online.org/front_content.php?idcat=1494.

0277-3791/$ – see front matter © 2012 Elsevier Ltd. All rights reserved.
doi:10.1016/j.quascirev.2012.05.012

Despite technical and logistical difficulties and in order to better understand the geomagnetic field variability, a series of paleomagnetic records from the mid- to high-latitudes of the Southern Hemisphere (from 30°S to Antarctica) emerged in the last decade. The available high-resolution paleomagnetic records are often limited to the Holocene and deglacial period and include sediment drifts near Antarctica (Brachfeld et al., 2000; Willmott et al., 2006) and lacustrine sediments from Argentina (e.g., Gogorza et al., 2002, 2004, 2006; Irurzun et al., 2006). In addition, a very high-resolution record from offshore Chile covers the last 70 ka cal BP (Kaiser et al., 2005; Lund et al., 2006b). Other records from the Southern Hemisphere extending back to the last glacial period are however at lower temporal resolutions (e.g., Atlantic sector of the Southern Ocean, Stoner et al., 2002, 2003; Indian sector of the southern Ocean, Mazaud et al., 2002; near Antarctica: Macrì et al., 2005, 2010; Scotia Sea, Collins et al., 2012; Lake Pupuke in New Zealand, Nilsson et al., 2011).

In southern Argentina, the absence of a continental glacier over the Pali Aike Volcanic Field during the last glaciation (Zolitschka et al., 2006; Coronato et al., 2013) suggests a continuous accumulation of sediment in the maar lake Laguna Potrok Aike, and previous studies indicate high sedimentation rates of ca 100 cm/ka since 16 ka cal BP (Haberzettl et al., 2007). Therefore Laguna Potrok Aike is a key site for high-resolution paleomagnetic reconstruction in the mid-latitudes of the Southern Hemisphere. Previous paleomagnetic studies from the sediments of Laguna Potrok Aike include a series of short cores covering the last 0.7 ka cal BP (Gogorza et al., 2011) and the full vector paleomagnetic record for the last 16 ka cal BP was reconstructed as part of the South Argentinean Lake Sediment Archives and modelling (SALSA) project (Gogorza et al., 2012). A low-resolution rock-magnetic study from that lake recently revealed that no major change in the magnetic mineral assemblage occurred since the last glacial period (Recasens et al., 2011). Here we present a high-resolution rock-magnetic study of the lacustrine sediments and a continuous full-vector paleomagnetic record since 51.2 ka cal BP from a continental archive in the mid-latitudes of the Southern Hemisphere in order to document the variability of the geomagnetic field in an area of the world where observations are scarce.

2. Geological setting

Laguna Potrok Aike (51°58′S, 70°22′W) is a maar lake within the Pali Aike Volcanic Field in the province of Santa Cruz in southern Argentina. The Pali Aike volcanic field is a series of phreatomagmatic craters formed by back-arc volcanism since the Pliocene to the Pleistocene (Corbella, 2002; Zolitschka et al., 2006; Coronato et al., 2013). Laguna Potrok Aike is today a perennial lake in the Patagonian steppe, with a maximum water depth of 100 m and a maximum diameter of 3.5 km. The lake is fed by groundwater with no inflow or outflow at present (Mayr et al., 2007); however, gullies (visible in Fig. 1) indicate episodic inflow most likely related to snowmelt events. In addition, lake level terraces above and below the present lake level document the sensitivity of the lake system to hydrological changes (Haberzettl et al., 2008; Anselmetti et al., 2009; Gebhardt et al., 2012). Laguna Potrok Aike is influenced by the strong Southern Hemisphere westerly winds (SHW) and as a result the water column is not stratified or well-oxygenated from top to bottom (Zolitschka et al., 2006). The lake is located at ca 100 km from the Atlantic coast and ca 200 km on the lee-side of the Andes, where the annual precipitation is less than 300 mm/yr (Zolitschka et al., 2006). These geomorphological and geographical settings suggest that the terrigenous sediment enters the lake by eolian input and periodic runoff. The sources of the detrital sediment deposited in Laguna Potrok Aike are 1) the Andean Cordillera and the derived fluvioglacial sediments, tills and moraines deposited in the catchment area before the Late Pleistocene, and 2) the basaltic lavas and volcanic structures such as maars, tuff-rings, scoria and spatter cones in the Pali Aike Volcanic Field (D'Orazio et al., 2000; Zolitschka et al., 2006; Ross et al., 2011; Coronato et al., 2013).

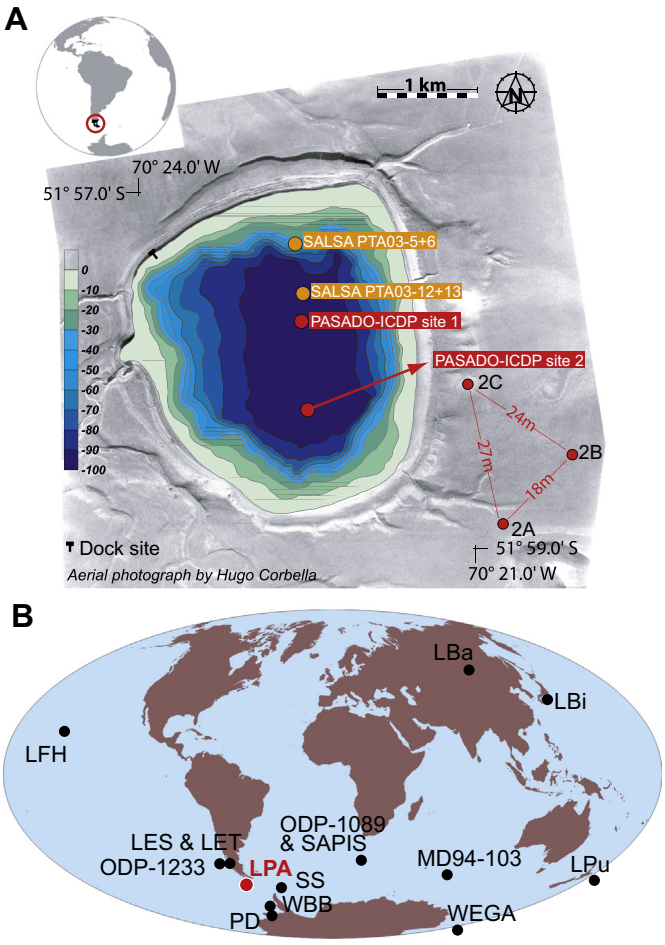

Fig. 1. A) Aerial photograph and bathymetry of the maar lake Laguna Potrok Aike in the Patagonian steppe of southern Argentina. The position of the PASADO-ICDP sites 1 and 2, the holes at site 2 and the SALSA records discussed in the text are indicated. B) Location of the paleomagnetic records discussed in the text. From west to east, LFH: Lava flow stack from Hawaii (Teanby et al., 2002), ODP-1233: Ocean Drilling Program core 1233 offshore Chile (Lund et al., 2006b), LEs & LEt: Lake Escondido and Lake El Trébol (Gogorza et al., 2002, 2004, 2006; Irurzun et al., 2006), LPA: Laguna Potrok Aike (Gogorza et al., 2012; this work), WBB: Western Bansfeld Basin (Willmott et al., 2006), PD: Palmer Deep (Brachfeld et al., 2000), SS: Scotia Sea stack (Collins et al., 2012), ODP-1089 & SAPIS: Ocean Drilling Program core 1089 (Stoner et al., 2003) and stack of the sub-Antarctic South Atlantic Ocean (Stoner et al., 2002), WEGA: Wilkes Land Basin stack (Macrì et al., 2005), LBa: Lake Baikal (Peck et al., 1996), LBi: Lake Biwa (Hayashida et al., 2007), LPu: Lake Pupuke (Nilsson et al., 2011).

3. Methods

3.1. Coring and sampling

The PASADO-ICDP scientific drilling operations at Laguna Potrok Aike were completed during the austral spring 2008 (September to November). The PASADO science team recovered 533 m of azimuthally unoriented sediment cores from 2 sites using a piston coring system supported by a barge (GLAD800) and operated by the Consortium for Drilling, Observation and Sampling of the Earth's Continental Crust (DOSECC) (Zolitschka et al., 2009; Kliem et al., 2013). Site 2 was selected for high-resolution multi-proxy analyses because of its higher recovery rate (98.8%) and its apparent

lower proportion of sands compared to site 1. The composite profile of site 2 (2CP; 106.09 m composite depth (cd)) was constructed by correlating the lithology of parallel cores from three holes (Fig. 1) (Kliem et al., 2013). The 2CP was continuously sampled with u-channels (2 × 2 cm section plastic liner) following the method of Stoner and St-Onge (2007) at the University of Bremen in June 2009. A total of 98 u-channels (maximum length of 1.5 m) were sampled, with the exception of section 85 which contained gravel (2A-30H-2; from 8813 to 8896 cm cd). Here we present the results of the pelagic sediments, which represent 43% (45.8 m) of the 2CP. The remaining 57% (60.29 m) was identified as reworked material from mass movement deposits (Kliem et al., 2013; see Section 3.5 Lithology below). Finally, the core catcher samples from hole A at site 2 (position on Fig. 1) as well as discrete samples (ca 2–3 g) collected at ca 40 cm-interval along the 2CP were used for rock-magnetic investigation.

3.2. Continuous magnetic measurements

The magnetic measurements of the 2CP u-channel samples were performed at 1 cm-interval at the *Institut des sciences de la mer de Rimouski* (ISMER). The low-field volumetric magnetic susceptibility (k_{LF}) was measured using a point sensor mounted on a multi sensor core logger (MSCL) and the natural remanent magnetisation (NRM) was measured using a 2G cryogenic magnetometer for u-channels. Because of the edge effect associated with the response function of the cryogenic magnetometer pick-up coils (Weeks et al., 1993), 4-cm of data were not used on both sides of intersections and stratigraphic gaps. Likewise, unreliable points linked to incompletely filled u-channels, disturbed sediment and outlier values were not considered for the paleomagnetic reconstruction. A minimum of 13 demagnetisation steps (0, 5, 10, 15, 20, 25, 30, 35, 40, 45, 50, 60, 70 mT) were used to progressively demagnetise the initial NRM to less than 20%. The paleomagnetic inclination and declination as well as the associated maximum angular deviation (MAD) values were calculated from the characteristic remanent magnetisation (ChRM) interval using principal component analysis (Kirschvink, 1980) in the Excel spreadsheet developed by Mazaud (2005). The cores were not azimuthally oriented and hence the declination values were "un-rotated" to obtain a continuous record and each section was centered to zero. An anhysteretic remanent magnetisation (ARM) was imparted with a peak alternating field (AF) of 100 mT and a direct current (DC) biasing field of 0.05 mT, then demagnetised and measured in a minimum of 8 steps (0, 10, 20, 30, 40, 50, 60, 70 mT). Afterwards two isothermal remanent magnetisations ($IRM_{300\ mT}$ and $IRM_{950\ mT}$) were induced using a 2G pulse magnetiser and step-wise demagnetised using the same method as for the ARM. The $IRM_{950\ mT}$ is used as the saturation isothermal remanent magnetisation (SIRM). The susceptibility of the ARM (kARM) is calculated by dividing the ARM with the biasing DC field applied and is commonly used to establish a magnetic grain size indicator such as kARM/SIRM (e.g., Stoner and St-Onge, 2007) or kARM/k (e.g., Banerjee et al., 1981; King et al., 1982). The median destructive field (MDF) of the remanent magnetisations (e.g., MDF_{NRM}, MDF_{ARM} and MDF_{IRM}) were calculated in order to determine the required applied field to remove half of the initial remanence. It is a measure of the coercivity of the remanence carriers and hence depends on the magnetic mineralogy and grain size. When the magnetic mineralogy is uniform, the MDF informs on the magnetic grain size of the magnetic recording assemblage.

3.3. Discrete magnetic measurements

A total of 103 discrete pelagic sediment samples were measured using a Princeton Measurement Corporation alternating gradient force magnetometer (model MicroMag 2900 AGM) in order to obtain the hysteresis curves and derived properties, including the bulk coercive force (Hc), the remanent coercive force (Hcr), the saturation magnetisation (Ms) and the saturation remanence (Mr). The isothermal remanent magnetisation (IRM) acquisition curve was also acquired for 43 samples using the same instrument. The coercivity (Hcr/Hc) and the remanence (Mr/Ms) ratios are commonly used as magnetic grain size indicators (Day et al., 1977; Dunlop, 2002) and the hysteresis properties, together with the IRM acquisition curve, inform on the coercivity of the remanence carriers (Dunlop and Özdemir, 1997, 2007). In order to further investigate the magnetic mineralogy, the temperature-dependence of magnetic susceptibility (k_T) was measured for all core catcher samples of hole A site 2 using a Bartington MS2 κ/T system with the ceramic crucible filled at full capacity (ca 3 g). Recasens et al. (2011) showed that 4 core catcher samples from hole A site 2 are dominated by reworked tephra (samples 21, 22 and 27CC) or organic-rich (sample 6CC) material and were readily identifiable by rock-magnetic properties. The present study focuses on the pelagic sedimentation and therefore the remaining core catcher samples from hole A site 2 were considered. Mineralogical analysis of typical core catcher samples (samples 10, 12 and 28CC) was conducted using a Siemens D5000 X-Ray diffractometer at the X-ray diffraction laboratory of UQAM. The bulk sediment was sieved to isolate the grain size fractions <38 μm and between 38 and 106 μm. For each size fraction a magnetic extract was obtained using a rare earth neodymium hand magnet. This method is rapid, but less efficient in collecting the smaller magnetic grains and it is therefore not quantitative (Hounslow and Maher, 1999). The semi-quantitative mineralogical identification was conducted by diffraction peak analysis (based on Bragg's law) using the International Center for Diffraction Data (ICDD) database as a reference.

3.4. Chronology

The chronology of the event-corrected PASADO 2CP pelagic sediment sequence (45.80 m cd-ev) is based on 36 radiocarbon dates and supported with 6 tephra layers (see Kliem et al., 2013 for details; Table 1; Fig. 2). It is also supported by lithological and tephra correlation with previously studied cores from Laguna Potrok Aike, including a core located nearby in the lake center and covering the last 16 ka cal BP (PTA03/12 + 13; location on Fig. 1; Haberzettl et al., 2007) and a low-resolution core from a lake level terrace covering a similar time span (PTA03/5 + 6; location on Fig. 1; Haberzettl et al., 2009).

3.5. Lithology

Kliem et al. (2013) described five lithological units for the sediment of Laguna Potrok Aike since 51.2 ka cal BP. The units are based on the type of pelagic sediment and the frequency of mass movement deposits (MMD) and include (A) pelagic laminated silts, (B) pelagic laminated silts intercalated with thin fine sand and coarse silt layers, (C-1, C-2 and C-3) alternation of A and B with an increase in the frequency and thickness of MMD from C-1 to C-3. The present work concerns exclusively the pelagic sediment from these different units (see the log on Figs. 4 and 7).

4. Results

4.1. Magnetic mineralogy

The isothermal remanent magnetisation (IRM) acquisition curves of the 43 pelagic sediment samples (Fig. 3A; position on Fig. 4) reach saturation below ca 200 mT, indicating a magnetic

Table 1
AMS radiocarbon ages for the PASADO-ICDP site 2 sedimentary record from Laguna Potrok Aike (modified from Kliem et al., 2013). The ages are calibrated with CalPal applying the CalPal_2007_HULU calibration curve. Ages from reworked sediment sections are printed in bold.

Laboratory no.	Sample description	Sediment depth (m cd)	Event corrected sediment depth (m cd–ec)	^{14}C Age (BP)	Error (1σ)	Calibrated age (cal BP)	Error (1σ)
Poz-834[a]	Stems of aquatic moss	0.51	0.51	440	30	510	30
Poz-897[a]	Bulk sediment	0.56	0.55	655	25	630	50
Poz-3570[a]	Calcite fraction of bulk sample	0.67	0.67	735	25	690	20
Poz-896[a]	Stems of aquatic moss	0.92–1.04	0.92–1.04	1470	40	1370	40
Poz-5182[b]	Twig of Berberis	1.96	1.95	2300	35	2290	70
Poz-8549[b]	Calcite fraction of bulk sample	2.88	2.87	3600	35	3910	50
Poz-8390[b]	Stems of aquatic moss	3.10–3.15	3.10–3.15	3625	35	3940	50
Poz-8398[b]	Stems of aquatic moss	4.83	4.53	4465	50	5130	120
Poz-8550[b]	Calcite fraction of bulk sample	6.00	5.71	6440	70	7360	60
Poz-8391[b]	**Stems of aquatic moss**	6.91	6.63	7025	50	7870	60
Poz-8546[b]	Calcite fraction of bulk sample	8.12	7.83	7260	50	8090	60
Poz-8392[b]	Stems of aquatic moss	9.69	9.37	7580	50	8390	40
Poz-8393[b]	**Stems of aquatic moss**	10.44	9.97	9640	50	11000	140
Poz-8547[b]	**Calcite fraction of bulk sample**	11.00–11.08	10.53–10.61	9410	50	10640	60
Poz-8394[b]	**Stems of aquatic moss**	12.00	11.37	11090	60	12980	80
Poz-5985[b]	Bone of Tuco Tuco	13.04	12.22	8930	50	10060	110
Poz-8548[b]	Calcite fraction of bulk sample	14.78	13.00	10240	60	11970	130
Poz-8396[b]	Stems of aquatic moss	15.55	13.78	11200	60	13130	80
Poz-8397[b]	Stems of aquatic moss	16.40	14.61	12490	70	14900	140
Poz-5072[b]	**Stems of aquatic moss**	16.78–18.20	14.70	12850	70	15420	90
Poz-5073[b]	Stems of aquatic moss	18.48–18.54	14.93–14.99	13450	70	16710	100
Poz-37017[c]	Stems of aquatic moss	18.69	15.13	14540	70	17760	50
Poz-37022[c]	Stems of aquatic moss	22.09	16.74	17460	80	20970	120
Poz-37007[c]	Stems of aquatic moss	23.25	17.90	18700	120	22570	110
Poz-32491[c]	**Stems of aquatic moss**	23.90	18.23	27910	240	32420	280
Poz-34233[c]	**Stems of aquatic moss**	26.65	19.42	22450	140	27230	320
Poz-37020[c]	Stems of aquatic moss	27.20	19.69	20490	120	24510	150
Poz-37008[c]	Stems of aquatic moss	31.01	22.14	30300	300	34500	240
Poz-370103[c]	Organic macro remains	33.45	24.46	47000	2000	50590	2670
Poz-34235[c]	**Stems of aquatic moss**	35.10	25.49	26930	210	31720	140
Poz-34236[c]	Stems of aquatic moss	36.38	26.67	25110	180	30030	170
Poz-34237[c]	Stems of aquatic moss	36.66	26.95	25820	190	30750	320
Poz-32492[c]	**Stems of aquatic moss**	39.77	28.69	34500	500	39770	910
Poz-37011[c]	Stems of aquatic moss	40.09	28.98	29300	300	33700	350
Poz-37012[c]	Organic macro remains	45.81	30.30	31900	300	35780	380
Poz-37002[c]	Stems of aquatic moss	47.34	31.34	29600	300	33930	310
Poz-37013[c]	Stems of aquatic moss	48.58	32.32	40000	1000	43730	810
Poz-34238[c]	Stems of aquatic moss	52.98	32.82	37300	800	42040	500
Poz-37003[c]	Stems of aquatic moss	53.12	32.96	39200	700	43140	570
Poz-32493[c]	**Stems of aquatic moss**	54.23	33.88	27680	230	32230	230
Poz-37014[c]	**Stems of aquatic moss**	54.23	33.88	44000	2000	47450	2200
Poz-37075[c]	Stems of aquatic moss	55.59	34.15	30800	400	34920	380
Poz-34239[c]	Stems of aquatic moss	56.66	34.71	42000	2000	45610	1850
Poz-34240[c]	Stems of aquatic moss	58.91	36.00	43000	2000	46510	2040
Poz-34241[c]	Stems of aquatic moss	63.18	36.70	50000	3000	53610	3630
Poz-37018[c]	Organic macro remains	65.11	37.33	43000	2000	46510	2040
Poz-32494[c]	Stems of aquatic moss	67.13	38.87	43000	2000	46510	2040
Poz-34242[c]	Stems of aquatic moss	72.80	40.56	44000	2000	47450	2200
Poz-37004[c]	Stems of aquatic moss	73.32	40.66	47000	2000	50590	2670
Poz-34243[c]	**Stems of aquatic moss**	75.18	41.40	47000	2000	50590	2670
Poz-37006[c]	Stems of aquatic moss	75.68	41.67	51000	4000	53910	4130
Poz-37021[c]	Organic macro remains	78.43	42.39	>48000			
Poz-32495[c]	Stems of aquatic moss	80.60	42.97	45000	2000	48430	2320
Poz-34245[c]	Stems of aquatic moss	96.21	45.71	>48000			
Poz-37015[c]	Organic macro remains	96.21	45.71	52000	4000	54580	3940
Poz-37016[c]	Organic macro remains	98.95	45.79	42000	1000	45200	1060
Poz-34246[c]	**Stems of aquatic moss**	99.89	45.80	50000	4000	53220	4250
Poz-32496[c]	**Stems of aquatic moss**	102.96	45.80	>45000			

[a] Haberzettl et al. 2005.
[b] Haberzettl et al. 2007.
[c] Kliem et al., 2013.

assemblage dominated by low coercivity minerals. The median destructive field of the natural remanent magnetisation (MDF_{NRM}; Fig. 4) and the coercive force (Hc; not shown) vary around average values of 16 mT and 7.2 mT, respectively. Along with the typical shape of the hysteresis loop (Fig. 3C) (Tauxe et al., 1996), these results are characteristic of magnetite. Furthermore, zero magnetic susceptibility is reached during heating at or near the Curie temperature of magnetite (580 °C; Dunlop and Özdemir, 1997, 2007) for the 22 core catcher samples of site 2 hole A (Fig. 3B). A drop in magnetic susceptibility slightly before 580 °C suggests the presence of Ti-poor titanomagnetite (Dearing, 1999). However, the diffractogram of the magnetic extracts further identifies magnetite as the dominant magnetic mineral both in the grain size fraction 106–38 μm and <38 μm (Fig. 3C). Altogether these results support the previous magnetic mineral analyses for the last 16 ka cal BP (Gogorza et al., 2011, 2012) as well as the low-resolution analyses of

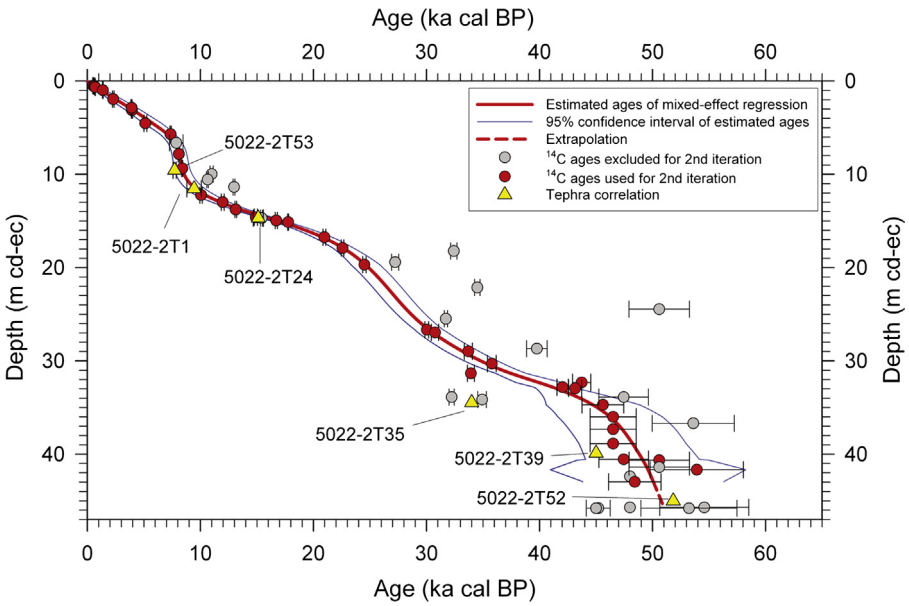

Fig. 2. Radiocarbon-based age model for the PASADO-ICDP site 2 sedimentary record (modified from Kliem et al., 2013). The composite depth event-corrected (cd-ec) corresponds to the depth after removal of mass movement deposits and it represents the pelagic sediment sequence. The red line is the estimated age after two iteration of the mixed-effect regression using the constant-variance function (for more details, see Kliem et al., 2013). (For interpretation of the references to colour in this figure legend, the reader is referred to the web version of this article.)

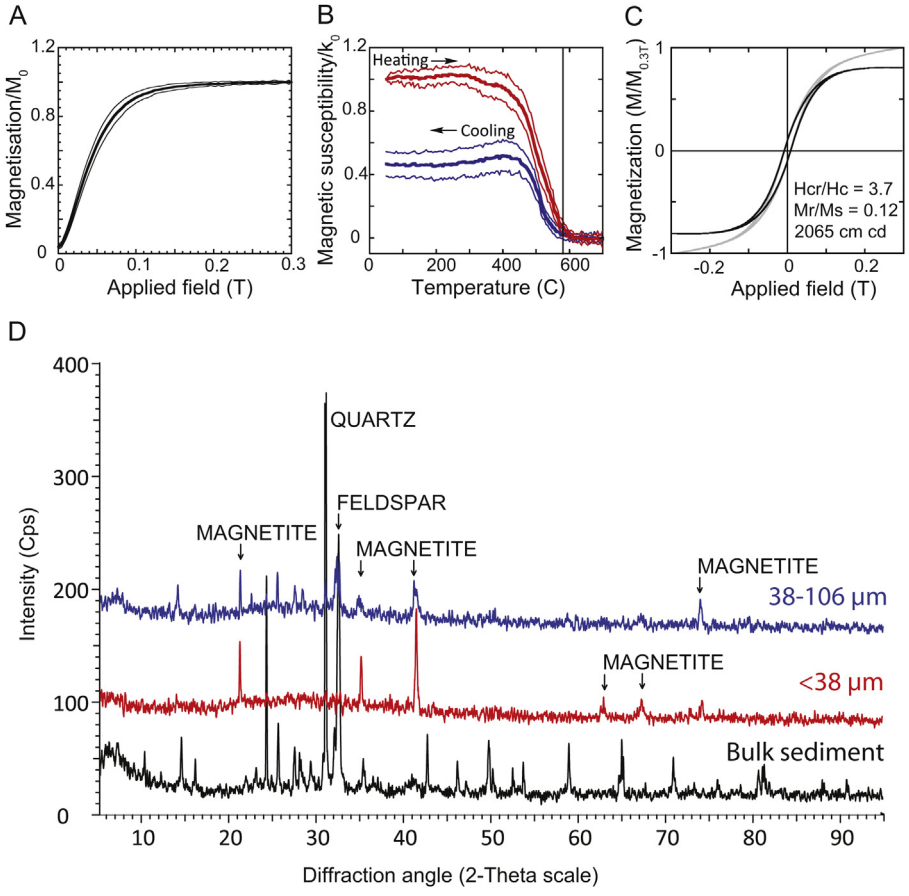

Fig. 3. A) Average isothermal remanent magnetisation (IRM) acquisition curves of 43 pelagic samples from the composite profile at site 2. The IRM is normalized with the value in an applied field of 0.3 T. B) Average heating (red) and cooling (blue) curves of the magnetic susceptibility for 22 core catcher samples at site 2 hole A. The magnetic susceptibility is normalized with the initial value (at 50 °C). The standard deviation (thin lines) are shown for A and B. C) Hysteresis curve for a typical sample. The raw (grey) and high-field slope corrected (black) magnetisation are illustrated. D) Typical X-ray diffraction spectrum for the bulk sediment and for magnetic extracts (sample 2A–12CC). The curves for the magnetic extracts (38–106 µm and <38 µm) were shifted vertically for clarity. The rock-magnetic and mineralogical analyses indicate that magnetite dominates the magnetic mineral assemblage at Laguna Potrok Aike. (For interpretation of the references to colour in this figure legend, the reader is referred to the web version of this article.)

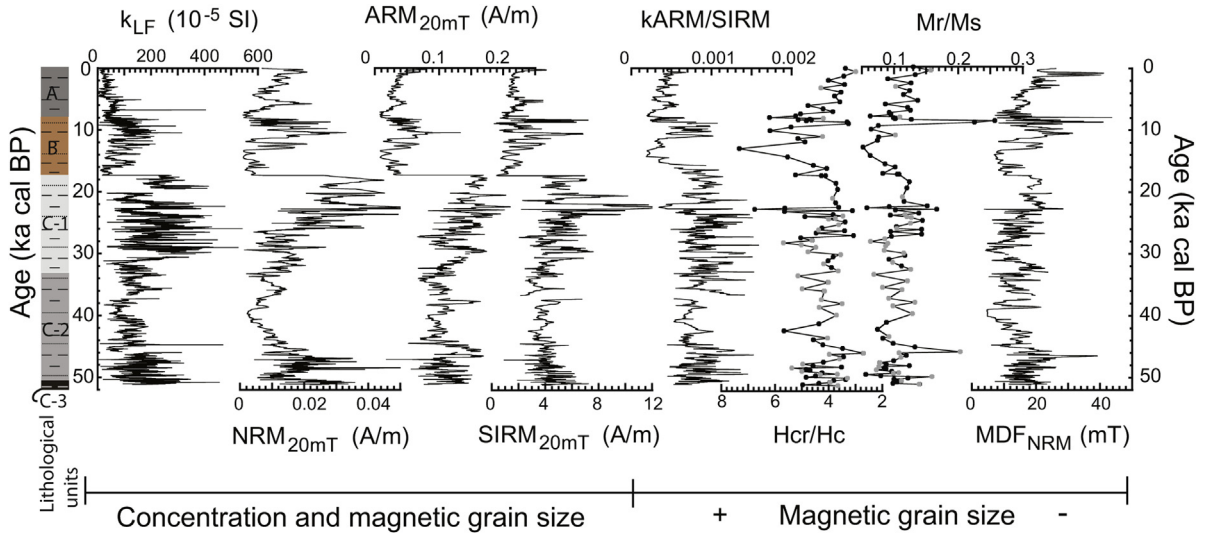

Fig. 4. Rock-magnetic properties of the pelagic sediments at Laguna Potrok Aike since 51.2 ka cal BP. A) The low-field magnetic susceptibility (k_{LF}), the natural remanent magnetisation ($NRM_{20\ mT}$) and the anhysteretic and isothermal remanent magnetisations after 20 mT demagnetisation ($ARM_{20\ mT}$, $IRM_{20\ mT}$) are influenced by the concentration and the grain size of the magnetic minerals; kARM/SIRM, Hcr/Hc, Mr/Ms and MDF_{NRM} reflect grain size changes for a magnetic assemblage dominated by magnetite. Samples analyzed for IRM acquisition curves are indicated by a grey symbol. The lithological units from Kliem et al. (2013) are located on the left hand side. The log represents the pelagic sediments only, after removal of the mass movement deposits. Unit A: Pelagic laminated silts prevail; almost no mass movement deposits. Unit B: Dominance of pelagic laminated silts intercalated with thin fine sand and coarse silt layers; normal graded units and ball and pillow structures occur; high content of plant macro remains and gastropods. Unit C-1: Dominance of pelagic laminated silts intercalated with thin fine sand and coarse silt layers; normal graded units and ball and pillow structures occur. Unit C-2: Dominance of normal graded units and ball and pillow structures among pelagic laminated silts intercalated with thin fine sand and coarse silt layers. Unit C-3: Dominance of normal graded units, ball and pillow structures, sand and gravel layers; a few pelagic laminated silts intercalated with thin fine sand and coarse silt layers occur.

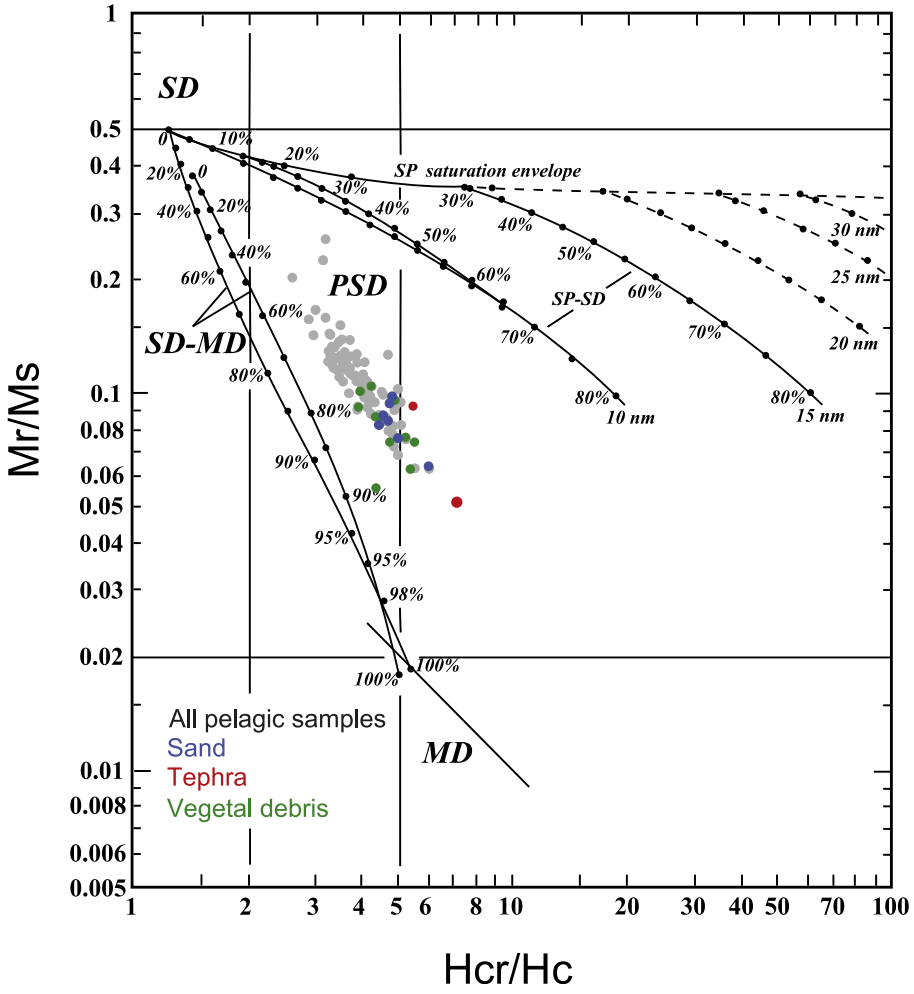

Fig. 5. Day plot (Day et al., 1977) for the pelagic sediment samples of Laguna Potrok Aike since 51.2 ka cal BP. The mixing reference lines for single and multi-domain (SD and MD) are from Dunlop (2002).

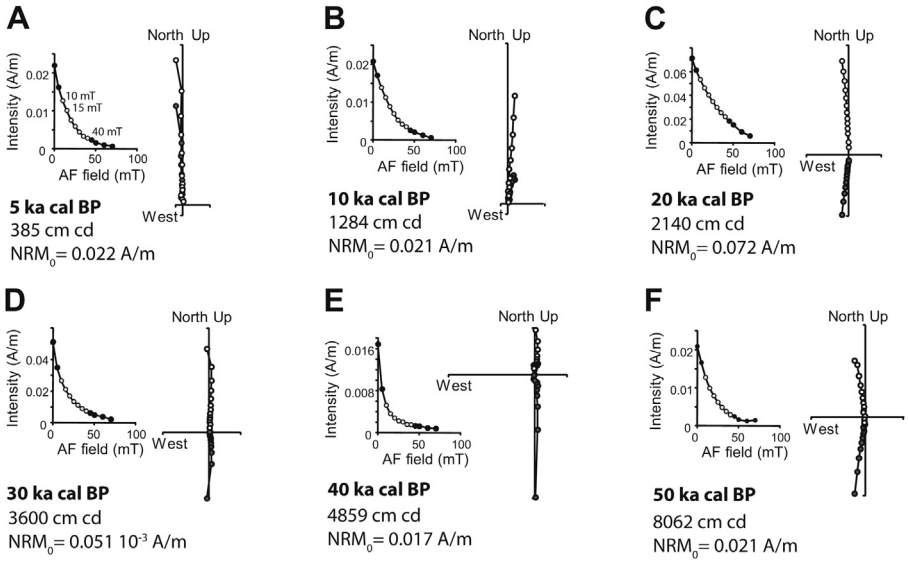

Fig. 6. Typical demagnetisation curves and orthogonal projections for the pelagic sediment from Laguna Potrok Aike at A) 5 ka cal BP, B) 10 ka cal BP, C) 20 ka cal BP, D) 30 ka cal BP, E) 40 ka cal BP, F) 50 ka cal BP. The characteristic remanent magnetisation (ChRM) interval (from 10 to 40 mT demagnetisation steps) is represented with light grey symbols. The open (closed) symbols in the vector end-point orthogonal diagram represent the projection in the vertical (horizontal) plane.

the PASADO-ICDP core catcher samples (Recasens et al., 2011) and reveal that magnetite is the dominant remanence carrier at Laguna Potrok Aike since 51.2 ka cal BP.

4.2. Magnetic concentration

The natural remanent magnetisation (NRM) of sediments is influenced by the intensity of the Earth's magnetic field at the moment of deposition and by lithological factors such as the mineralogy, the concentration and the grain size of the magnetic carriers (Tauxe, 1993). Fig. 4 presents the NRM after 20 mT demagnetisation along with the magnetic grain size and concentration proxies since 51.2 ka cal BP. While the magnetic susceptibility and the remanent magnetisations (NRM, ARM, IRM) depend on both the concentration and the magnetic grain size, the ratio kARM/SIRM, Hcr/Hc and Mr/Ms, as well as MDF_{NRM}, reflect changes in grain size (e.g., Dunlop and Özdemir, 1997; Stoner and St-Onge, 2007 and references herein). The similarity of the curves clearly illustrates the influence of the magnetic concentration and grain size on the NRM, as expected for a magnetic mineralogy dominated by magnetite.

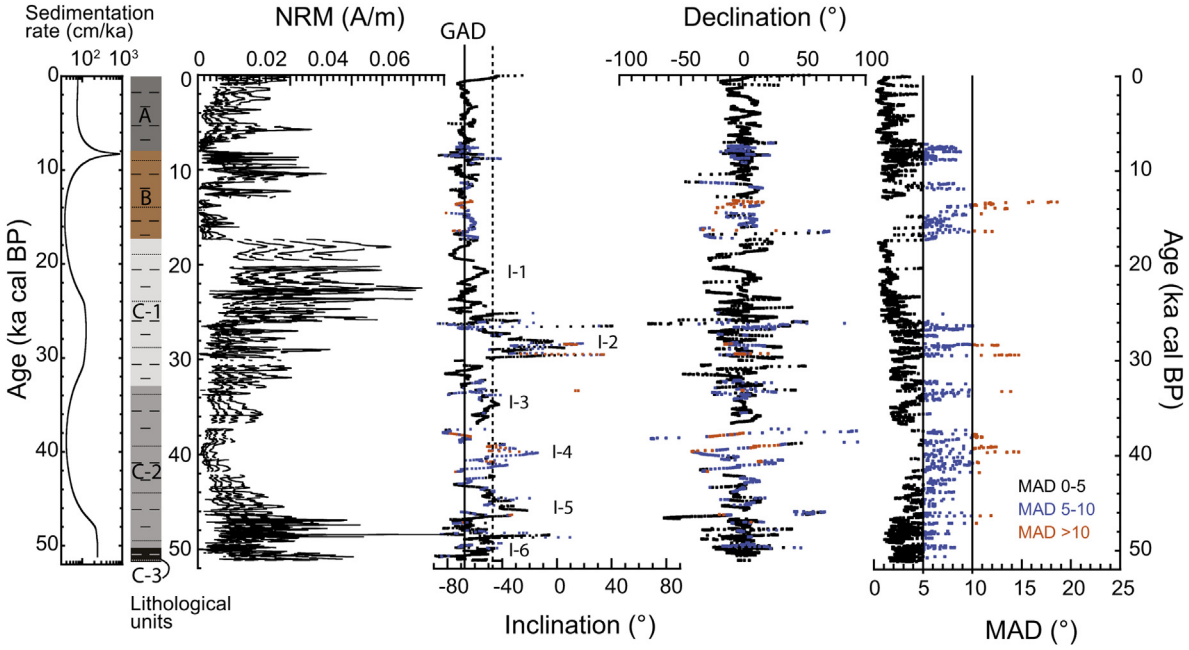

Fig. 7. Paleomagnetic directions recorded at Laguna Potrok Aike since 51.2 ka cal BP. From left to right: the natural remanent magnetisation (NRM) at the demagnetisation steps 10, 20, 30 and 40 mT, the paleomagnetic inclination, declination and the maximum angular deviation (MAD) values calculated for the characteristic remanent magnetisation (ChRM) interval from 10 to 40 mT (7 steps). The continuous vertical line on the inclination graph is the geocentric axial dipole (GAD) value at the coring site. Intervals of low inclinations are indicated (I-1 to I-6; see text for details) and the dashed line represent a departure of 20° from the GAD. The sedimentation rates and the lithological units from Kliem et al. (2013) are located on the left hand side. For the description of the lithological units A, B, C-1, C-2 and C-3, the reader is referred to Fig. 4.

The more notable rock-magnetic change is a sharp diminution in the concentration of magnetic minerals at 17.3 ka cal BP, and is observed in all concentration-dependant parameters (k_{LF}, NRM, ARM, IRM) (Fig. 4). The concentration change at 17.3 ka cal BP is coeval with a sharp increase of the total organic carbon (TOC) (Hahn et al., 2013; Recasens et al., 2011; Zhu et al., 2013) and it represents the limit between the lithological units C-1 and B (Fig. 4), where plant macro remains and gastropods become abundant (Kliem et al., 2013). Hence the diminution in the magnetic concentration proxies most likely reflects the dilution of magnetic minerals by increased organic sediments. This transition corresponds to the onset of the last deglaciation in the Southern Hemisphere (Schaefer et al., 2006). The maximum change in the concentration of magnetic minerals for the PASADO-ICDP 2CP record is of approximately one order of magnitude (see the concentration-dependant parameters in Fig. 4), which is commonly considered as a maximal range for a high quality paleomagnetic study (Tauxe, 1993).

4.3. Magnetic grain size

The grain size proxies vary with similar amplitudes throughout the record (Fig. 4). Nonetheless, there is a gradual coarsening trend from 18 to 12 ka cal BP followed by a slight trend towards finer magnetic grains during the Holocene. These results suggest that no drastic change occurred in the grain size of the remanence carriers since 51.2 ka cal BP. This is supported with the coercivity and remanence ratios (Hcr/Hc and Mr/Ms) used in a "Day plot" to estimate the domain state of the magnetic grains (Day et al., 1977) (Fig. 5). All 103 samples fall in and to the right of the region indicative of pseudo-single domain (PSD) magnetite and also align parallel to the theoretical single and multi-domain (SD + MD) mixing line for magnetite (Dunlop, 2002). The samples in which sand, tephra and/or vegetal debris were visually identified (20 samples) plot to the right of the cluster (Fig. 5). This suggests that these particular and easily identifiable samples contain a higher proportion of MD magnetite grains or a contribution of other magnetic minerals. On the other hand, the rest of the samples are dominated by PSD magnetite, which is optimal for paleomagnetic recording (King et al., 1983; Tauxe, 1993; Stoner and St-Onge, 2007).

4.4. Paleomagnetic directions

A strong and stable single-component magnetisation is isolated from 10 mT to 40 mT (7 demagnetisation steps) and is identified as the characteristic remanent magnetisation (ChRM) (Fig. 6). A viscous magnetisation, if present, is easily removed after 5 or 10 mT demagnetisation. The NRM at the demagnetisation steps 10, 20, 30 and 40 mT only are presented in Fig. 7 for clarity. The ChRM MAD values are generally $\leq 5^\circ$ (81% of the data), indicating a well-defined component magnetisation for Quaternary sediments (Stoner and St-Onge, 2007). The data associated with MAD values between 10° and 5° (17%) and >10° (2%) generally correspond to intervals with relatively low NRM and MDF, most likely indicating coarser PSD magnetic grains and/or a lower concentration of magnetic minerals. However, these intervals are still relatively well-defined with MAD values generally <15° (Butler, 1992; Opdyke and Channell, 1996) and they are not systematically associated to inclination values departing significantly from the theoretical value considering a geocentric axial dipole (GAD; −68°, indicated with a vertical line on Fig. 7). The average inclination value is −67° for the last 17.3 ka cal BP and −55° for the period from 51.2 to 17.3 ka cal BP. The average inclination value during the last glacial period is lower than the GAD value and results from a series of intervals with lower inclinations (I-1 to I-6; Fig. 7). There is no systematic inclination shallowing that would be attributed to geological recording (Tauxe, 2005). The inclination lows I-1, I-3 and I-6 depart up to approximately 20° from the GAD value (vertical dashed line in Fig. 7), whereas I-2, I-4 and I-5 depart more than 20° from the GAD. Flattening by post-depositional compaction induced by frequent mass movement deposits (MMD) at Laguna Potrok Aike could account for low inclinations (Anson and Kodama, 1987; Tauxe, 2005) and a greater effect of compaction on the inclination record would be expected with depth, where the number and thickness of the MMD are higher (Kliem et al., 2013). This is not the case and for example, the deepest pelagic sediment recovered within the stratigraphic unit characterised by thick and numerous MMD (C-3; Kliem et al., 2013) recorded an average inclination of −64°, which is near the GAD value.

I-2 is the interval displaying the lowest inclination values. It is found from 30 to 27 ka cal BP and positive inclination values are reached. The inclination abruptly shifts to low values at 30 ka cal BP and progressively returns to the GAD value at ca 27 ka cal BP. This large feature represents 4 m of pelagic sediments and corresponds to a period of high sedimentation rates (Fig. 7; Kliem et al., 2013) with an average of 133 cm/ka. This interval corresponds to a period of extended land exposure associated with an absence of terminal lakes in Patagonia (Sugden et al., 2009) and may correspond to a period of low lake level during which a major unconformity was formed on the lake shoulder (Gebhardt et al., 2012). Even though an environmental influence might appear likely, the magnetic grain size indicators in this interval reveal only a mild increase that does not differ from the average values (Fig. 4) and altogether the rock-magnetic results support a genuine geomagnetic recording. A flattening of the inclinations by compaction during a period of high sedimentation rates could induce low inclinations. However, no relation is found between the sedimentation rates and the inclination values at Laguna Potrok Aike (Fig. 7) and similar high-sedimentation rates previously allowed the recording of excellent paleomagnetic records (>100 cm/ka; e.g., St-Onge et al., 2003; Stoner et al., 2007; Lisé-Pronovost et al., 2009). In addition, the two periods with the highest sedimentation rates (from 51.2 to 46.3 and from 9.4 to 6.6 ka cal BP) display inclination values around the GAD value, further supporting a genuine geomagnetic signal. An alternative explanation for the low inclinations of the interval 30–27 ka cal BP is linked to the observation that this sedimentary interval was difficult to correlate between the two overlapping holes (A and C). For example, one tephra layer was present in one hole (part of the composite depth) but absent in the other. Therefore although a stable and well-defined ChRM associated with MAD values lower than 10 (average of 8.3°) and carried by PSD magnetite suggest a genuine geomagnetic origin of the paleomagnetic direction, the possibility of a large and undetected synsedimentary deformation (e.g., Channell and Stoner, 2002) cannot be excluded. There are no sedimentary structures suggesting deformation (for more detail see Kliem et al., 2013) and without additional evidence, the interval 30–27 ka cal BP is considered pelagic; however the paleomagnetic record in this interval should be regarded with caution.

The two other intervals with inclinations deviating more than 20° from the GAD are I-4 and I-5. I-4 represents the interval from 41.5 to 38.7 ka cal BP with a minimum inclination recorded at 39.8 ka cal BP (−14°). This interval represents 1.03 m of sediment and the sedimentation rates are lower (37 cm/ka) relative to the average since 51.2 ka cal BP at Laguna Potrok Aike. Sharp and large amplitude declination changes are associated with this interval, as well as distinctively low NRM values (Fig. 4), while the other concentration-dependant parameters do not present such a minimum. In addition, this interval is characterized by relatively low MDF_{NRM} (<10 mT; Fig. 4) and MAD values >5° (Fig. 7), thus suggesting the presence of coarser PSD magnetic grains, also illustrated by a rapid decrease of

the NRM during step-wise demagnetisation (Fig. 6E). Coarse MD magnetite grains are generally poor recorder of the geomagnetic field (Tauxe, 1993). However the rock-magnetic result still indicate PSD domain state and as other intervals with similar rock-magnetic properties (NRM, MDF, and MAD) display inclinations values around the GAD value (e.g., ca 17–11 and 9–7 ka cal BP), directions in this interval are considered reliable.

I-5 is the interval from 46.7 to 43.5 ka cal BP and is characterised by a sharp shallowing of the inclination to values around −50°, followed by a sharp return around the GAD value at 43.5 ka cal BP. Large amplitude changes in declination are also observed from 47 to 46 ka cal BP. It represents ca 2.08 m of sediment deposited with a mean sedimentation rate of 65 cm/ka. Like all the other intervals departing from the GAD value during the last glacial period, the rock-magnetic results support a genuine geomagnetic origin of the signal.

4.5. Relative paleointensity

The natural remanent magnetisation (NRM) carried by sediments is a detrital remanent magnetisation (DRM). In order to build a relative paleointensity proxy (RPI), it is assumed that the DRM is proportional to the paleo field (Tauxe, 1993). However, changes in the concentration, grain size and mineralogy of the magnetic grains can additionally affect the natural remanence. Therefore the NRM is commonly normalised using a rock-magnetic parameter, typically ARM, IRM or k_{LF}. Because k_{LF} is measured in the presence of an applied field, it is not only influenced by concentration and grain size changes, but also by grains that do not contribute to the DRM, including coarse MD grains, diamagnetic and paramagnetic material. For this reason k_{LF} should be used with caution and here we use ARM and IRM.

The relative paleointensity estimates using ARM and IRM as normalisers of the NRM yield similar results. In order to identify the appropriate normaliser, two different normalisation methods were compared for each paleointensity estimate using the UINT software (Xuan and Channell, 2009) (Fig. 8A and B). The average ratio method is widely used (e.g., Stoner et al., 2003; Barletta et al., 2008; Lisé-Pronovost et al., 2009) and is built by averaging the normalized NRM at different demagnetisation steps. Here we use four demagnetisation steps (10, 20, 30 and 40 mT) of the characteristic remanent magnetisation interval (ChRM). The pseudo Thellier method or the slope method (Tauxe et al., 1995; Channell et al., 2002; Snowball and Sandgren, 2004; Xuan and Channell, 2009) uses the slope of the NRM versus the normaliser at different demagnetisation steps, here at 10, 20, 30 and 40 mT. The two methods give similar results for $NRM/ARM_{10–40\ mT}$ and the correlation coefficient (R) calculated from the slope method are high (average $R = 0.997$; dotted line in Fig. 8A), suggesting a close resemblance of the NRM and ARM coercivity spectrum. In contrast, the two methods of paleointensity estimate using IRM as a normaliser ($NRM/IRM_{10–40\ mT}$; Fig. 8B) are different for several intervals, notably for the last 4000 cal BP. In addition, the correlation coefficients are systematically lower for $NRM/IRM_{10–40\ mT}$ and present more scatter and sharp minima (Fig. 8B). Furthermore, the MDF_{NRM} is best correlated with the MDF_{ARM} ($R = 0.42$) than with the MDF_{IRM} ($R = 0.07$), indicating that the grains acquiring the ARM more closely match the coercivity of the grains carrying the natural remanence (Levi and Banerjee, 1976). This is also illustrated by looking at the demagnetisation behaviour of NRM, ARM and IRM for the entire pelagic sediment record, where ARM better matches the behaviour of the NRM than IRM (Fig. 8C). This figure illustrates in a continuous way the remaining magnetisation after each demagnetisation steps 10, 20, 30 and 40 mT. The demagnetisation behaviour is clearly more variable for the IRM than for the NRM and ARM.

Coherence tests of the best relative paleointensity estimate ($NRM/ARM_{10–40\ mT}$) with its normaliser were achieved for the average ratio and slope methods following the Tauxe and Wu (1990) method and using the software Analyseries (Paillard et al., 1996) (Fig. 9A). The relative paleointensity estimates $NRM/ARM_{10–40\ mT}$ using the ratio and slope methods are superimposed and there is coherence at some frequencies (Fig. 9A), hinting at a possible environmental overprint. Most of the periods where coherence is observed are from 100 to 200 years, illustrating high-frequency secular variations possibly not normalized adequately and thus lithological in origin. However, only very few periods (>300 yr) are coherent at the secular to millennial and millennial timescales, suggesting that both RPI estimates are geomagnetic in origin at these timescales. In addition, these few frequencies are not significant in the power spectrum of neither the RPI estimates, or for the normalisers (Fig. 9A). Nevertheless, the source of the high-frequency environmental overprint was investigated, identified and is illustrated in Fig. 9B where a good correspondence of the RPI estimates with MDF_{NRM} is observed. Correlation coefficients (R) of 0.58 and 0.41 for the ratio and slope methods, respectively, suggest a grain size influence on the RPI

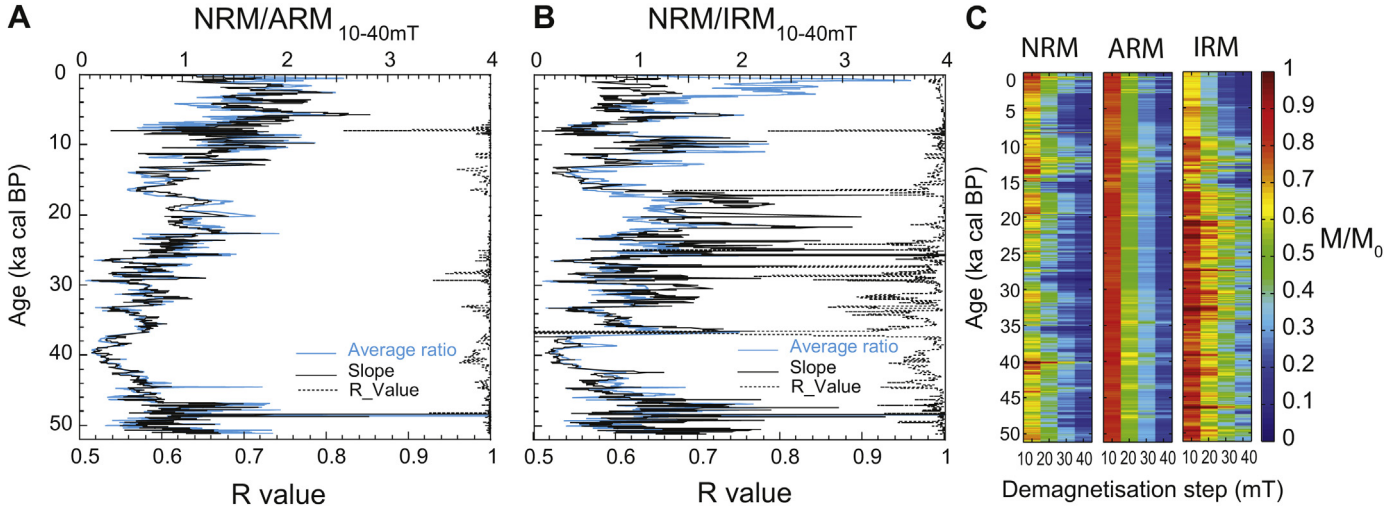

Fig. 8. Comparison of the relative paleointensity estimates A) $NRM/ARM_{10–40\ mT}$ and B) $NRM/IRM_{10–40\ mT}$ using the average ratio and the slope methods. C) Demagnetisation behaviour of the NRM, ARM and IRM at 10, 20, 30 and 40 mT demagnetisation steps. The colour scale represents the magnetic remanence (M) normalized by the value before step-wise demagnetisation (M_0). (For interpretation of the references to colour in this figure legend, the reader is referred to the web version of this article.)

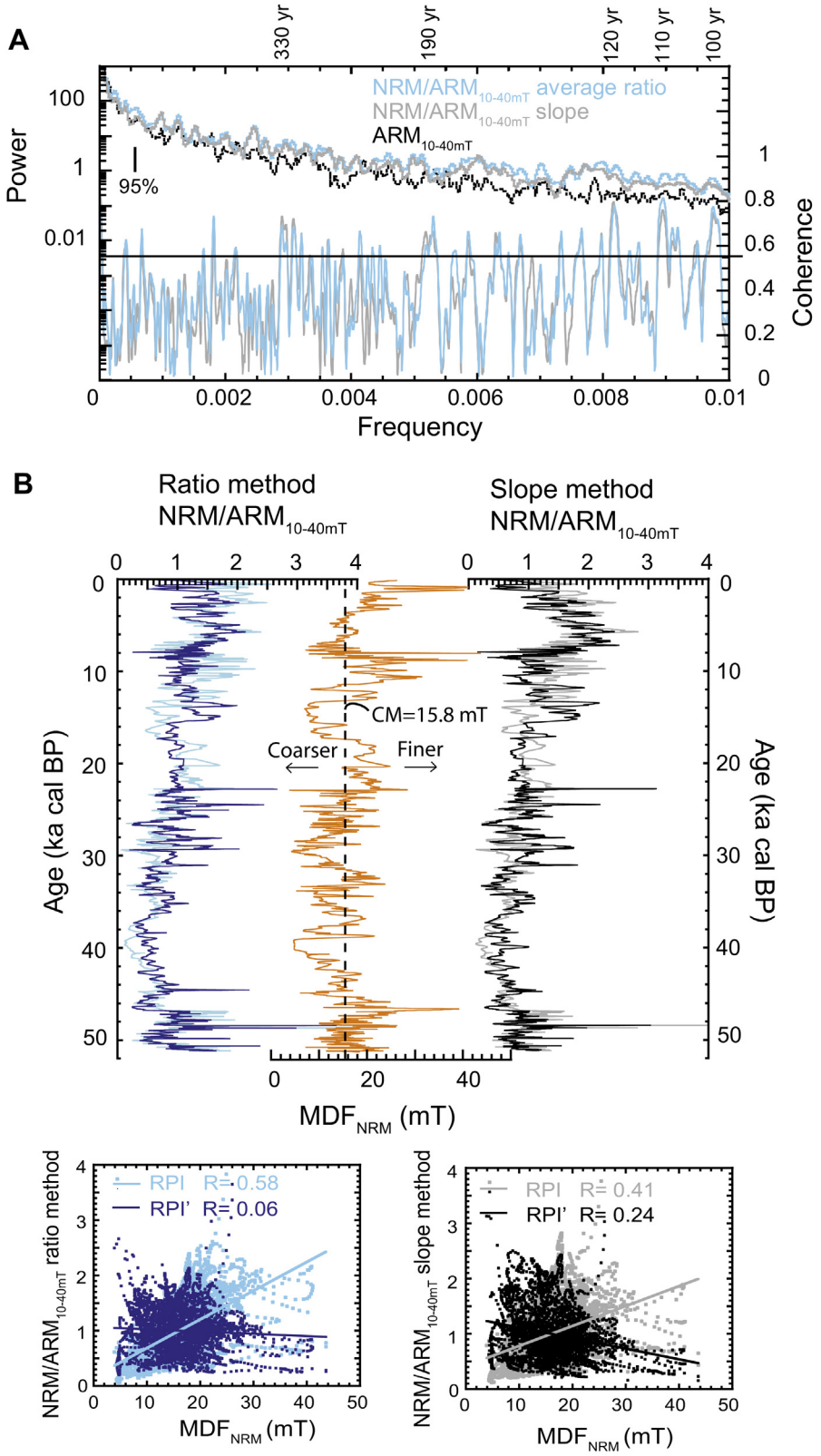

Fig. 9. A) Coherence tests of the relative paleointensity estimate NRM/$ARM_{10–40\ mT}$ with its normaliser using the Blackman–Tukey method with a Bartlett window. The solid horizontal line represents the level above which the coherence is significant at the 95% confidence. B) Relative paleointensity estimates using the average ratio and the slope methods before (RPI) and after (RPI') the secondary normalisation using MDF_{NRM} to account for magnetic grain size influence on DRM (see text for details). CM is the center of mass and represents the median MDF_{NRM} value. The scatter plots in inset reveal that the correlation is significantly reduced for both methods and the NRM/$ARM_{10–40\ mT}$ average ratio is not correlated with the MDF_{NRM}.

estimates. In order to correct for that grain size influence and to obtain the best possible RPI proxy, a secondary normalisation was applied to both RPI estimates by using a correction factor used previously by Brachfeld and Banerjee (2000) to remove the grain size influence on the RPI estimate of Holocene sediments from Lake Pepin (Minnesota, USA). Brachfeld and Banerjee (2000) revealed that this simple correction can be used effectively to correct a paleomagnetic signal overprinted by grain size changes. The correction is based on the linear relationship between the paleointensity estimate (RPI) and MDF_{NRM} using the equation:

$$RPI' = RPI \times MDF_{NRM-CM}/MDF_{NRM}$$

where $MDF_{NRM\text{-}CM}$ is the center of mass of the MDF_{NRM}, which is determined from the RPI vs. MDF_{NRM} scatter plot (median value of 15.8 mT; Fig. 9B). The correction simply adjusts the amplitude of the RPI variations to account for the non-geomagnetic effect of coercivity changes on the RPI. Therefore, intervals of greater difference between the RPI and RPI' (corrected intervals) correspond to the minimum and maximum values of the MDF_{NRM}. Considering that the MDF_{NRM} is a grain size proxy for the sediments of Laguna Potrok Aike (Fig. 4), coarser (finer) magnetite grains underestimate (overestimate) the relative paleointensity. The greater corrections are found for the intervals 41–38, 30–28, 16–13, 11–8 and 3–0 ka cal BP (Fig. 9B). Finally, the correlation of the RPI' with the magnetic grain size proxy MDF_{NRM} is significantly reduced for both RPI estimates (average ratio and slope; Fig. 9B), and especially for the average ratio method ($R = 0.06$). Therefore, the preferred RPI proxy for the PASADO-ICDP record is $NRM/ARM_{10-40\ mT}$ calculated using the average ratio method.

The RPI proxy presented here fulfils the required criteria for high quality record from sediments (King et al., 1983; Tauxe, 1993; Stoner and St-Onge, 2007), including 1) a single, strong and well-defined ChRM (Fig. 6) carried by PSD magnetite (Figs. 3, 4 and 5), 2) no inclination error (Fig. 7), 3) the variation in the concentration of magnetic minerals is limited to approximately one order of magnitude (Fig. 4), 4) similar RPI estimates are obtained from different normalization methods (Fig. 8), 5) the RPI proxy is independent of bulk rock-magnetic parameters after a secondary normalization using MDF_{NRM} (Fig. 9), 6) there is a good agreement of the paleomagnetic record with the closest available records (Fig. 11; see below).

5. Discussion

5.1. Paleomagnetic secular variations and geomagnetic excursions

Changes of the virtual geomagnetic pole by less than 40–45° are commonly referred to as geomagnetic secular variation and greater changes, also associated to low geomagnetic intensity, are considered as geomagnetic excursions (e.g., Merrill and McFadden, 1994; Laj and Channell, 2007; Roberts, 2008). In the last 52 ka cal BP, the Laschamp (40.7 ± 1 ka cal BP; Singer et al., 2009) and Mono Lake (32.4 ± 0.3 ka cal BP, Singer, 2007) geomagnetic excursions are the only two recognized geomagnetic excursion and they are believed to occur globally (Laj and Channell, 2007). They are however not always recorded because of their short durations, which are estimated from the cosmogenic isotope records from Greenland to 1.2 and 2.5 kyr, for the Mono Lake and Laschamp geomagnetic excursion, respectively (Wagner et al., 2000). Therefore, the capability of recording geomagnetic excursions depends on the sedimentation rate, the lock-in depth and the associated post-depositional remanent magnetisation (PDRM) smoothing (Roberts and Winklhofer, 2004). In the Southern Hemisphere, excursional geomagnetic directions associated with the Laschamp geomagnetic excursion were recorded from sedimentary archives in the Indian sector of the Southern Ocean (MD94–103; Mazaud et al., 2002) and offshore Chile with an unprecedented resolution (Ocean Drilling Program (ODP) site 1233; Table 2) (Lund et al., 2006a). At Laguna Potrok Aike, a large directional swing (I-4 and D-2; Fig. 10A and B) associated with the lowest relative paleointensity value recorded since 51.2 ka cal BP (Fig. 10C) is associated with the Laschamp geomagnetic excursion. The Mono Lake geomagnetic excursion was reported in southern South America at 35 ka cal BP in core ODP-1233 (Lund et al., 2006b), and elsewhere in the Southern Hemisphere at 31.6 ± 1.8 ka in lava flow of the Aukland volcanic field in New Zealand (Cassata et al., 2008). A low in inclination (I 3; Fig. 10A) and a minimum in RPI (Fig. 10C) at 34 ka cal BP could be associated with the Mono Lake excursion in the LPA record.

The major inclination low during the period 30–27 ka cal BP (I-2) is from pelagic sediment (Kliem et al., 2013) and the paleomagnetic results indicate excursional geomagnetic inclinations (Fig. 10A). Coeval sharp changes in inclination are observed in the ODP-1233 marine record from offshore Chile (Lund et al., 2006b), however with lower amplitude (Fig. 10A). An inclination low centered at ca 26 ka cal BP in the ODP-1089 marine record (Stoner et al., 2003) and the WEGA marine stack (Macrì et al., 2005) could further correspond to I-2 (Fig. 10A). Recently, Hodgson et al. (2009) reported a geomagnetic excursion at 26.8 ± 0.4 ka cal BP from the former subglacial Lake Hodgson in Antarctica (72°00′S, 68°29′W; 2200 km distance from LPA) and tentatively linked it to the Mono Lake excursion. If I-2 corresponds to the Mono Lake excursion (32.4 ± 0.3 ka cal BP, Singer, 2007), it would imply that "too young" ages are attributed to the sediment of Laguna Potrok Aike in this interval. This is unlikely for a radiocarbon-based chronology; however we note that no radiocarbon ages contribute to the age model in this specific interval (from 30.03 to 27.23 ka cal BP; Kliem et al., 2013). The strongest argument against the interpretation of I-2 being the Mono Lake excursion, however, is the absence of a coeval declination swing (Fig. 10B) and of a relative paleointensity minimum (Fig. 10C), as would be expected during a geomagnetic excursion. Instead, the large inclination swing I-2 at Laguna Potrok Aike is associated with the intensity maxima R-4. Hence I-2 is interpreted either as 1) a regional feature of the field, or 2) associated with an undetected synsedimentary deformation.

A directional swing at ca 20 ka cal BP is recorded around southern South America (LPA, ODP-1233 and ODP-1089) and identified as I-1 and D-1 (Fig. 10A and B). This feature is associated with a local low in paleointensity from Laguna Potrok Aike (Fig. 10C), as well as from global dipole estimates such as the GEOMAGIA dipole model (Knudsen et al., 2008) and the marine stack GLOPIS-75 (Laj et al., 2004) (Fig. 12C). Interestingly, this feature could correspond to the Hilina Pali geomagnetic excursion, recorded with details during times of intense volcanic activity in Hawaii at ca 20 ka cal BP (Laj et al., 2002; Teanby et al., 2002). Excursional directions at 18–22 cal BP were also reported from Eastern Arctic cores (Nowaczyk and Knies, 2000; Nowaczyk et al., 2003), Lake Baikal in Siberia (Peck et al., 1996) and lava flows from Amsterdam Island, southeastern Indian Ocean (Carvallo et al., 2003). However, the age for this feature is often poorly constrained and Xuan and Channell (2010) recently argued that the paleomagnetic inclination signal of Arctic sediments might be altered by diagenetic processes. To date, the geomagnetic excursion at 20 ka cal BP was only confidently dated in Hawaii. Nonetheless, a direction swing is recorded in southern South America at 20 ka cal BP and if it is associated to the geomagnetic excursion recorded 11,300 km away in Hawaii, it suggests a dominant feature of the field.

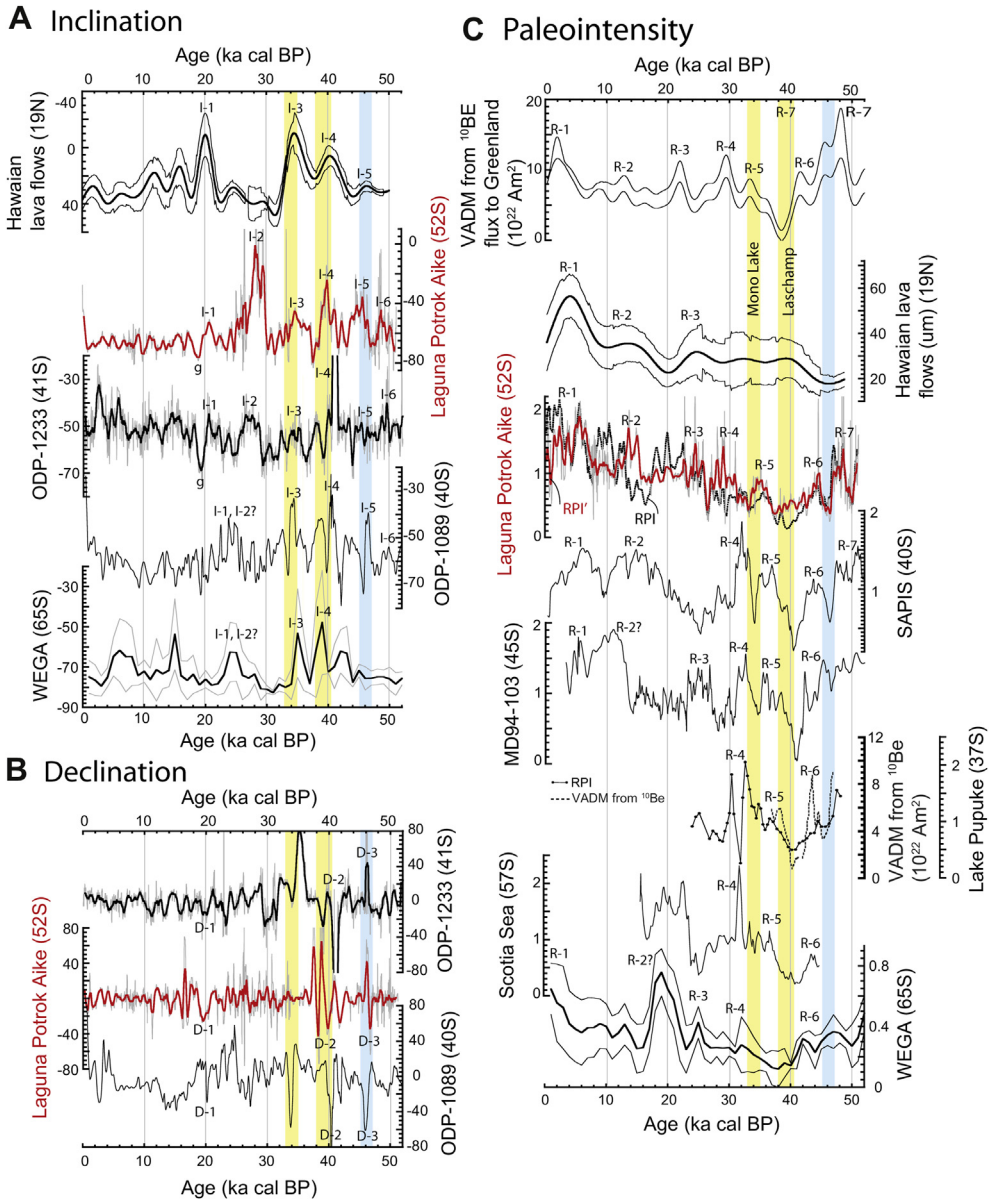

Fig. 10. Comparison of paleomagnetic A) inclination, B) declination and C) relative paleointensity records from the mid-to high-latitudes (37°–65°S) of the Southern Hemisphere since 52 ka cal BP. The virtual axial dipole moment (VADM) derived from the ^{10}Be flux to Summit, Greenland (Muscheler et al., 2005) and a lava flow compilation from Hawaii (Teanby et al., 2002) are also presented for comparison. The records include Laguna Potrok Aike in Patagonia (this study), the marine ODP-1233 core offshore Chile (Lund et al., 2006b), the marine ODP-1089 core (Stoner et al., 2003) and the SAPIS stack (Stoner et al., 2002) from the Atlantic sector of the Southern Ocean, the Scotia Sea stack (Collins et al., 2012), Lake Pupuke in New Zealand (RPI and VADM from ^{10}Be; Nilsson et al., 2011), the marine core MD93-104 from the Indian sector of the Southern Ocean (Mazaud et al., 2002), and the WEGA marine stack from the Wilkes Land Basin near Antarctica (Macrì et al., 2005). The thick lines represent the millennial variability of the high-resolution records (Laguna Potrok Aike and ODP-1233). The millennial-scale variability of the uncorrected (RPI) and corrected (RPI') relative paleointensity from Laguna Potrok Aike are also presented. Notable features of the paleomagnetic inclination (I-1 to I-6), declination (D-1 to D-3) and intensity (R-1 to R-7) are indicated. Note the reverse inclination axis for the Hawaiian lava flow compilation record located in the Northern Hemisphere. The Laschamp and Mono Lake geomagnetic excursions are underlined in yellow and the event at ca 46 ka cal BP in blue (see text for details). For the location of the records, please see Fig. 1B and Table 2. (For interpretation of the references to colour in this figure legend, the reader is referred to the web version of this article.)

5.2. Geomagnetic field variability in the Southern Hemisphere and in southern South America

Several directional features can be correlated among the records from the mid- to high-latitudes of the Southern Hemisphere, including most of the inclination lows (I-1, I-2, I-3, I-4, I-5, I-6) and the sharp declination swings (D-1, D-2, D-3) recorded at Laguna Potrok Aike (Fig. 10A and B). Similarly, a series of intensity high (R-1 to R-7) following the virtual axial dipole moment (VADM) record from the ^{10}Be flux to Greenland (Muscheler et al., 2005) can be identified in the records from the Southern Hemisphere (Fig. 10C). Some differences are also observed in the relative paleointensity records. All the records generally agree from 52 to 35 ka cal BP (R-7, R-6 and R-5; see also Fig. 11 of Kliem et al., 2013), however R-4 appears younger in LPA and in the VADM from Greenland. While the record from Laguna Potrok Aike is comparable to MD94-103 for the interval from ca 25 to 15 ka cal BP (including R-3, which is absent from SAPIS), it more closely resembles SAPIS since 15 ka cal BP (Fig. 10C).

The next step is to compare the new high-resolution full vector paleomagnetic record from Laguna Potrok Aike (LPA) to the available marine and lacustrine records around southern South America since 20 ka cal BP (Fig. 11), where more high-resolution

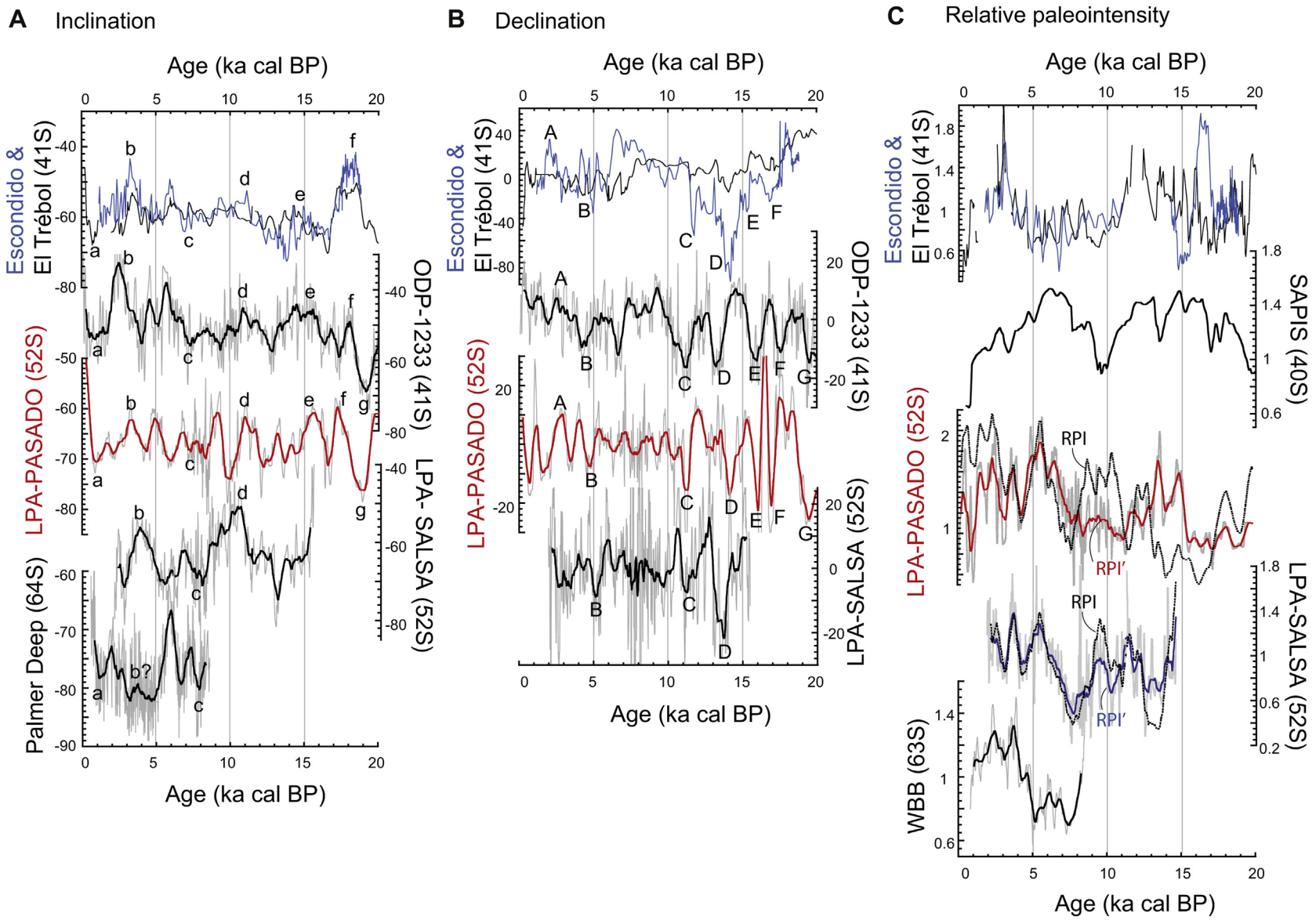

Fig. 11. Paleomagnetic A) inclination, B) declination, and C) relative paleointensity around Southern South America since 20 ka cal BP. The records are located from 40° to 64°S and include lake Escondido (Gogorza et al., 2002, 2004), lake El Trébol (Gogorza et al., 2006; Irurzun et al., 2006) and Laguna Potrok Aike (SALSA and PASADO projects, Gogorza et al., 2012 and this work) in Argentina, as well as marine records from offshore Chile (ODP-1233, Lund et al., 2006b), offshore the Antarctic Peninsula (WBB, Willmott et al., 2006; Palmer Deep, Brachfeld and Banerjee, 2000) and a stack from the sub-Antarctic South Atlantic (SAPIS; Stoner et al., 2002). The thick curves represent the millennial-scale variability of the high-resolution records (>80 cm/ka; Table 2). The millennial-scale variability of the uncorrected (RPI) and corrected (RPI') relative paleointensity from Laguna Potrok Aike are also presented. A set of correlative features for the inclination (a–g) and the declination (A–G) are indicated. Lake El Trébol is presented on the same graph as Lake Escondido because its chronology was established by magnetostratigraphy to Lake Escondido located less than 10 km away. The SAPIS stack is presented with the average data. All the records are presented on their own chronology and the PTA-SALSA record is plotted on the updated SALSA chronology from Kliem et al. (2013). For the location of the records, please see Fig. 1B and Table 2.

Table 2
Position, resolution and chronology of the paleomagnetic records presented in Figs. 10–12.

Record[a]	Distance from LPA (km)	Latitude	Longitude	Time period (kyr)	Sedimentation rate[b] (cm/ka)	Chronology	Reference[c]
Dipole moment							
VADM from ^{10}Be, Greenland	–	–	–	60–0	–	–	1
GEOMAGIA model	–	–	–	50–0	–	–	2
GLOPIS-75 (24 cores)	–	–	–	75–10	5–34.5	–	3
Lava flow							
LFH	11,330	19°29 N	154°54 W	45–0	–		4
Lacustrine records							
LPA-PASADO	–	51°37'S	69°10'W	51.2–0	89	36 ^{14}C	5
LPA-SALSA	–	51°37'S	69°10'W	16–0	84	16 ^{14}C, 1 tephra	6
LEs	1210	41°03'S	71°34'W	18.8–1.8	40	13 ^{14}C	7,8
LEt	1210	41°04'S	71°29'W	23.8–0.2	40	3 ^{14}C, magnetostratigraphy (inc and dec) with LEs	9,10
LBa	19,840	52°52'N	107°21'E	84–0.3	12	26 ^{14}C, 3 climatic tie-points	11
LBi	17,230	35°15'N	136°03'E	40–0	40	5 ^{14}C, 5 tephra	12
LPu	8320	36°47'S	174° 46'E	50–25	20	22 ^{14}C	13
Marine records and stacks							
ODP-1233	1260	41°00'S	74°24'W	70–0	170	24 ^{14}C, oxygen isotope stratigraphy	14
PD	1340	64°52'S	64°13'W	8.6–0.6	250	38 ^{14}C	15
WBB	1480	63°08'S	61°55'W	8.5–0.8	100	Magnetostratigraphy (RPI)	16
SS (2 cores)	1780	57°S	44°W	45–15.8	10	Magnetostratigraphy (RPI), diatom abondance stratigraphy	17
SAPIS (5 cores)	5970	41–47°S	6–10°E	80–0	15–25	ODP-1089 chronology	18
ODP-1089	5970	40°56'S	9°54'E	578–0.5	19	Oxygen isotope stratigraphy	19
MD94-103	8970	45°35'S	86°31'E	60–3.3	23	Magnetostratigraphy (RPI)	20
WEGA (6 cores)	6700	65°S	144°E	300–0	0.6–19	Magnetostratigraphy (RPI)	21

[a] The reader is referred to Fig. 1B for the complete name of the records and their position on the globe.
[b] The sedimentation rate is the average since 52 ka cal BP or for the complete record if it is younger.
[c] (1) Muscheler et al., 2005 (2) Knudsen et al., 2008 (3) Laj et al., 2004 (4) Teanby et al., 2002 (5) Kliem et al., 2013 (6) Haberzettl et al., 2007 (7) Gogorza et al., 2002 (8) Gogorza et al., 2004 (9) Irurzun et al., 2006 (10) Gogorza et al., 2006 (11) Peck et al., 1996 (12) Hayashida et al., 2007 (13) Nilsson et al., 2011 (14) Kaiser et al., 2005 (15) Brachfeld et al., 2000 (16) Willmott et al., 2006 (17) Collins et al., 2012 (18) Stoner et al., 2002 (19) Stoner et al., 2003 (20) Mazaud et al., 2002 (21) Macrì et al., 2005.

paleomagnetic records are available. The LPA-PASADO (this study) u-channel-based paleomagnetic record is in good agreement with the LPA-SALSA discrete samples-based record (Gogorza et al., 2012). Common directional paleomagnetic features are marked among the records from the southern South America region (<1500 km distance from LPA) (Fig. 11A and B). Some temporal shifts are observed and could be linked to the uncertainties of the respective chronologies (Table 2). Differences in the amplitude of variations could in turn be related to the different sedimentation rates and lock-in depths of the different records, as well as non-dipolar local features. A particularly good millennial-scale comparison is found between the paleomagnetic inclination (Fig. 11A) and declination (Fig. 11B) records of LPA-PASADO with the high-resolution marine record ODP-1233 from offshore Chile (Lund et al., 2006b). The majority of peaks and troughs can be readily correlated, including a large inclination swing preceding I-1 at ca 18 ka cal BP (from f to g), also visible in the records from Lake El Trébol (Irurzun et al., 2006) (Fig. 11A). Large declination swings, such as the features C, D, E, F and G (Fig. 11B), are also present in all the records from southern South America. All relative paleointensity records from the region (Fig. 11C) display relatively high values in the intervals 15–11 ka cal BP, followed by a decrease to lower values in the intervals 11–8 ka cal BP and 3–0 ka cal BP. However, the millennial-scale comparison is not straightforward, probably because of the variable quality of the available records. The highest resolution record (WBB; Willmott et al., 2006) is limited to 9 ka cal BP and the SAPIS stack should be treated with caution in the interval 20–0 ka cal BP because of a different magnetic assemblage (Stoner et al., 2002). The intervals 16–13, 11–8 and 3–0 ka cal BP were the most affected by the correction using MDF_{NRM} (Fig. 9B). Both the uncorrected and corrected RPI are presented in Fig. 11C and the better general fit of the corrected LPA-PASADO RPI record with the available regional records supports the use of this correction. In particular, a magnetic grain size influence on the RPI was successfully corrected in the interval 11–8 cal BP, where relatively smaller magnetite grains were inducing a peak (Fig. 9) that is not present in the other regional records (Fig. 11C). Overall, the full-vector paleomagnetic variability of the records from around southern South America is generally comparable at the millennial-scale since 20 ka cal BP.

5.3. Global-scale paleomagnetic intensity and direction comparison

The relative paleointensity record from Laguna Potrok Aike is compared with widely used dipole moment estimates since 52 ka cal BP from different types of archives (Fig. 12C). These records include the VADM derived from the ^{10}Be flux to Summit in Greenland (Muscheler et al., 2005), the marine stack GLOPIS-75 (Laj et al., 2004) and a dipole model based on archeomagnetic and volcanic data (GEOMAGIA dipole model; Knudsen et al., 2008). The records are generally consistent and most peak values of the dipole moment (R-1 to R-7) can be correlated among the records. Nonetheless, the global comparison reveals a marked difference at ca 46 ka cal BP. The inclination low event I-5 in Laguna Potrok Aike (Fig. 10A) is associated with the sharp declination swing D-3 (Fig. 10B) and a marked intensity low (Fig. 10C). Similar direction swing and intensity low are observed in the closest records (ODP-1233, Lund et al., 2006b; ODP-1089, Stoner et al., 2003) and the intensity low is observed at different degrees in numerous records from the Southern Hemisphere, including the Scotia Sea (Collins et al., 2012), the Sulu Sea (Schneider and Mello, 1996), the Indian and Atlantic sectors of the Southern Ocean (MD94-103; Mazaud et al., 2002, and SAPIS; Stoner et al., 2002), the western Equatorial Pacific (Blanchet et al., 2006), Lake Pupuke in New Zealand (Nilsson et al., 2011), and the WEGA stack near Antarctica (Macrì et al., 2005). This minimum in intensity is often absent or subdued in records from the Northern Hemisphere. For example, it represents a major difference between the NAPIS and SAPIS stacks in the interval 52–20 ka cal BP (Stoner et al., 2002). In addition, the

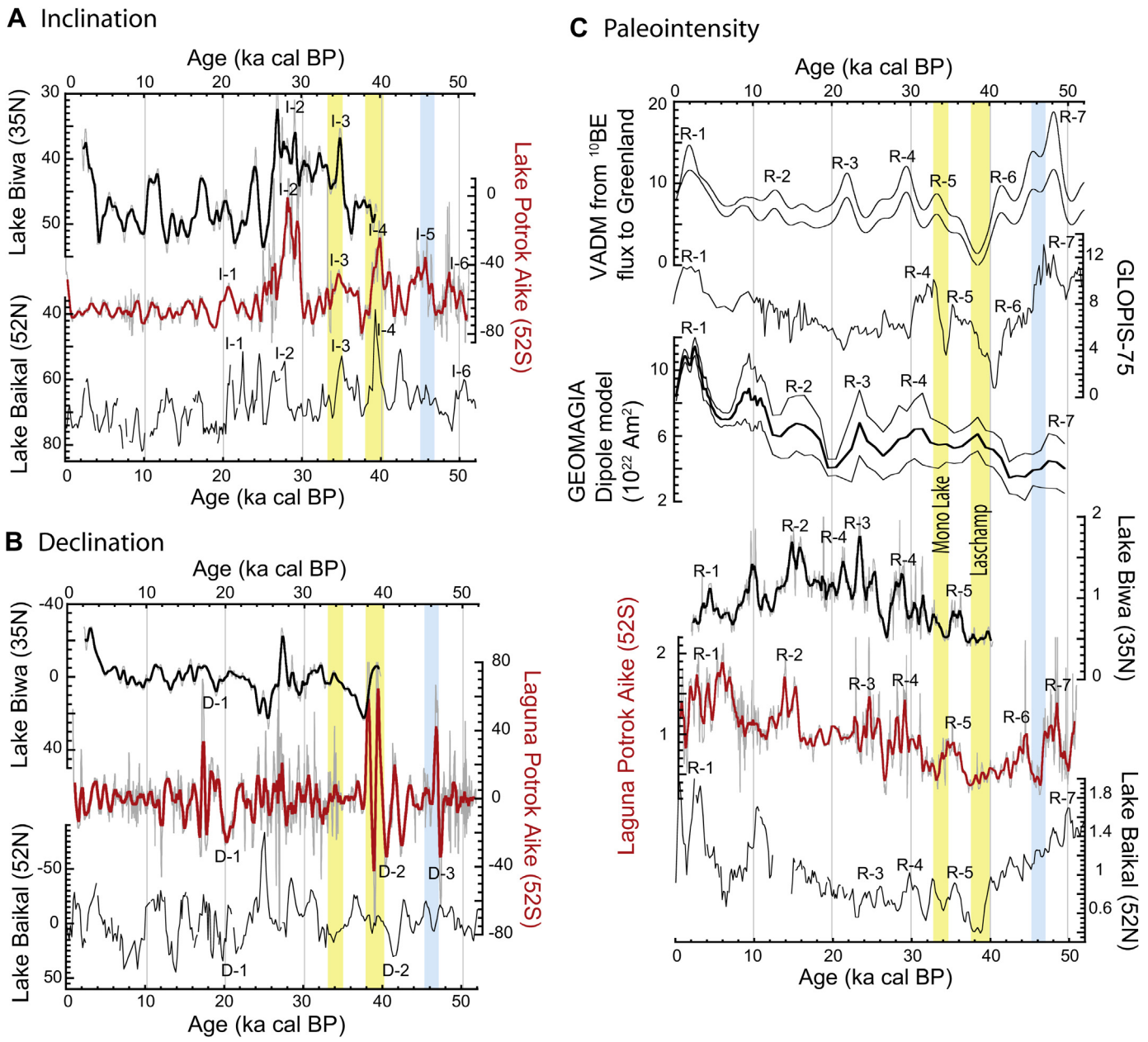

Fig. 12. Global-scale comparison of paleomagnetic A) inclination, B) declination and C) geomagnetic field intensity since 52 ka cal BP. The record from Laguna Potrok Aike (this study) is compared with the records from Lake Baikal in Siberia (Peck et al., 1996) and Lake Biwa in Japan (Hayashida et al., 2007). In addition, high-quality records of the dipole moment variability are presented and include the virtual axial dipole moment (VADM) derived from the ^{10}Be flux to Summit, Greenland (Muscheler et al., 2005), the marine stack GLOPIS-75 (Laj et al., 2004) and a model of the geomagnetic dipole based on absolute paleointensity data (Knudsen et al., 2008). The minimum and maximum VADM values from the ^{10}Be flux to Greenland are presented, the stack GLOPIS-75 with the average value and the GEOMAGIA dipole model with the average and error. Notable features of the paleomagnetic inclination (I-1 to I-6), declination (D-1 to D-3) and intensity (R-1 to R-7) are indicated. The Laschamp and Mono Lake geomagnetic excursions are underlined in yellow and the event at ca 46 ka cal BP in blue (see text for details). Note the reverse axis for the paleomagnetic directions of the records from the Northern Hemisphere. All the records are presented on their own chronology. For the location of the records, please see Fig. 1B. (For interpretation of the references to colour in this figure legend, the reader is referred to the web version of this article.)

records part of GLOPIS-75 and located in the Southern Hemisphere display this feature, but it was removed in the stack procedure, as most of the records were from the Northern Hemisphere (Laj et al., 2004). Therefore, the intensity low at 46 ka cal BP could represent an important Southern Hemisphere geomagnetic feature such as a possible analogue to the actual South Atlantic Anomaly, associated with a reverse flux patch at the core mantle boundary (e.g., Gubbins and Bloxham, 1985; Hulot et al., 2002). The South Atlantic anomaly (SAA) is a distinctive feature of the present field characterized at the surface of the Earth by a growing area of decreasing geomagnetic intensity since ca 400 years and currently located over South America (Hartmann and Pacca, 2009). The CALS10k.1b spherical harmonic model supports the recent character of the SAA, with Laguna Potrok Aike located within one of the two Southern Hemisphere high-flux patches when averaged over the last 10 ka (Korte et al., 2011).

Laguna Potrok Aike in the Southern Hemisphere (51°37′S, 69°10′W) is diametrically opposite to Lake Baikal in the Northern Hemisphere (52°51′N, 107°22′E). The geographical location of the two records on opposite sides of the Earth (Fig. 1B) is therefore ideal

to investigate the dipolar geomagnetic field since 51.2 ka cal BP. A full vector paleomagnetic comparison, including the LPA record, Lake Baikal (Peck et al., 1996) and a high-resolution record from Lake Biwa in Japan (Hayashida et al., 2007) is presented in Fig. 12. The comparison reveals a striking correlation of the inclination lows I-1, I-2, I-3, I-4, I-6, (with however different amplitudes for I-2 (Fig. 12A) and the declination swings D-1 and D-2 (Fig. 12B). As discussed previously, the directional feature (I-5 and D-3) associated with the intensity low at ca 46 ka cal BP (R-5) from LPA and other Southern Hemisphere records is absent from the Lake Baikal record in the Northern Hemisphere. All other relative paleointensity features are readily identified from the three records; however R-2 is missing from the Lake Baikal record, where there is a gap in the data. Furthermore, distinct peaks within each intensity maxima can be correlated between the high-resolution records from LPA and Lake Biwa, supporting the dipolar geomagnetic origin of these features for both records.

6. Conclusions

A new high-resolution rock-magnetic and paleomagnetic record was constructed from the long sedimentary archive of Laguna Potrok Aike (PASADO-ICDP) covering the last 51.2 ka cal BP. While the magnetic assemblage is dominated by PSD magnetite and remains stable from the last glacial period to the present interglacial, a marked decrease in the concentration of magnetic minerals at 17.3 ka cal BP is associated to the onset of the last deglaciation in Southern South America. A full vector paleomagnetic comparison of the Laguna Potrok Aike record with marine and lacustrine records from southern South America, other records from the mid- to high-latitudes of the Southern Hemisphere, and records located on the opposite side of the Earth as well as with global dipole moment reference curves 1) supports a genuine geomagnetic signal of the LPA-PASADO record, 2) generally supports the radiocarbon-based chronology (Kliem et al., 2013) at the millennial-scale, 3) verifies the global nature of the Laschamp and probably the Mono Lake geomagnetic excursion and 4) document distinct secular variations in southern South America at ca 20 and 46 ka cal BP, possibly reflecting important features of the past geomagnetic field. In particular, the directional swing and sharp minimum in intensity at 46 ka cal BP seem to be mainly observed in the Southern Hemisphere and could likely be used as a new regional chronostratigraphic marker. Finally, these new paleomagnetic results reveal magnetostratigraphy as a promising tool to better constrain the PASADO-ICDP chronology at least at the millennial-scale in specific intervals where geomagnetic changes are either global or regional.

Acknowledgements

We thank F. Barletta, J. Labrie, D. Veres, M.-P. St-Onge and A. Leclerc for their help in the laboratory at ISMER. We are grateful to L.G. Collins, A. Hayashida, P. Macri, A. Mazaud, R. Muscheler, A. Nillson, J. Peck, J. Stoner and N. Teanby for kindly sharing their data. This research is supported by the International Continental Scientific Drilling Program (ICDP) in the framework of the "Potrok Aike Maar Lake Sediment Archive Drilling Project" (PASADO). Funding for drilling was provided by the ICDP, the German Science Foundation (DFG), the Swiss National Funds (SNF), the Natural Sciences and Engineering Research Council of Canada (NSERC), the Swedish Vetenskapsradet (VR) and the University of Bremen. For their invaluable help in field logistics and drilling, we thank the staff of INTA Santa Cruz and Rio Dulce Catering as well as the Moreteau family and the DOSECC crew. This research was made possible through an NSERC Special Research Opportunity and Discovery grants to P. Francus and G. St-Onge. We also acknowledge the Canadian Foundation for Innovation (CFI) for the acquisition and operation of the u-channel cryogenic magnetometer. C. Gogorza thanks the *Comisión Nacional de Investigaciones Científicas y Técnicas de la República Argentina* (CONICET), the *Agencia Nacional de Promoción Científica y Tecnológica* (ANCyT) and the *Universidad Nacional del Centro de la Provincia de Buenos Aires* (UNCPBA). Finally, we acknowledge the support of NSERC and the Canadian Meteorological and Oceanographical Society (CMOS) for graduate scholarships to A. Lisé-Pronovost, and the *Fonds de recherche du Québec -Nature et technologies* (FQRNT) for a post-doctoral fellowship to T. Haberzettl.

References

Anselmetti, F.S., Ariztegui, D., De Batist, M., Gebhardt, C., Haberzettl, T., Niessen, F., Ohlendorf, C., Zolitschka, B., 2009. Environmental history of southern Patagonia unravelled by the seismic stratigraphy of Laguna Potrok Aike. Sedimentology 56, 873–892.

Anson, G.L., Kodama, K.P., 1987. Compaction-induced inclination shallowing of the post-depositional remanent magnetisation in a synthetic sediment. Geophys. J. Roy. Astr. Soc. 88, 673–692.

Banerjee, S.K., King, J., Marvin, J., 1981. A rapid method for magnetic granulometry with applications to environmental studies. Geophys. Res. Lett. 8, 333–336.

Barletta, F., St-Onge, G., Channell, J.E.T., Rochon, A., Polyak, L., Darby, D.A., 2008. High-resolution paleomagnetic secular variation and relative paleointensity records from the western Canadian Arctic: implication for Holocene stratigraphy and geomagnetic field behaviour. Can. J. Earth Sci. 45, 1265–1281.

Blanchet, C.L., Thouveny, N., de Garidel-Thoron, T., 2006. Evidence for multiple paleomagnetic intensity lows between 30 and 50 ka BP from a western Equatorial Pacific sedimentary sequence. Quat. Sci. Rev. 25, 1039–1052.

Brachfeld, S., Banerjee, S.K., 2000. A new high-resolution geomagnetic paleointensity record for the North American Holocene: a comparison of sedimentary and absolute intensity data. J. Geophys. Res. 105 (B1), 821–834.

Brachfeld, S., Acton, G.D., Guyodo, Y., Banerjee, S.K., 2000. High-resolution paleomagnetic records from the Palmer Deep, western Antarctic Peninsula. Earth Planet. Sci. Lett. 181, 429–441.

Butler, R.F., 1992. Paleomagnetism: Magnetic Domains to Geologic Terranes. Blackwell, Oxford.

Carvallo, C., Camps, P., Ruffet, G., Henry, B., Poidras, T., 2003. Mono Lake or Laschamp geomagnetic event recorded from lava flows in Amsterdam Island (southeastern Indian Ocean). Geophys. J. Int. 154, 767–782.

Cassata, W.S., Singer, B.S., Cassidy, J., 2008. Laschamp and Mono Lake geomagnetic excursions recorded in New Zealand. Earth Planet. Sci. Lett. 268, 76–88.

Channell, J.E.T., Stoner, J.S., 2002. Plio-Pleistocene magnetic polarity stratigraphies and diagenetic magnetite dissolution at ODP Leg 177 Sites (1089, 1091, 1093 and 1094). Mar. Micropaleontol. 45, 269–290.

Channell, J.E.T., Mazaud, A., Sullivan, P., Turner, S., Raymo, M.E., 2002. Geomagnetic excursions and paleointensities in the 0.9–2.15 Ma interval of the Matuyama Chron at ODP site 983 and 984 (Iceland Basin). J. Geophys. Res. 107 (B6), 1–11.

Collins, L.G., Hounslow, M.W., Allen, C.S., Hodgson, D.A., Pike, J., Karloukovski, V.V., 2012. Palaeomagnetic and biostratigraphic dating of marine sediments from the Scotia Sea, Antarctica: first identification of the Laschamp excursion in the Southern Ocean. Quat. Geochronol. 7, 67–75.

Corbella, H., 2002. El campo volcano-tectónico de Pali Aike. In: Haller, M.J. (Ed.), Geologiá y Recursos Naturales de Santa Cruz Relatorio del XV Congreso Geológico Argentino. El Calafate, Buenos Aires, pp. 287–303.

Coronato, A., Ercolano, B., Corbella, H., Tiberi, P., 2013. Glacial, fluvial and volcanic landscape evolution in the Laguna Potrok Aike Maar area, Argentina. Quat. Sci. Rev. 71, 13–26.

Day, R., Fuller, M., Schmidt, V.A., 1977. Hysteresis properties of titano-magnetite: grain size and compositional dependence. Phys. Earth Planet. Int. 13, 260–267.

D'Orazio, M., Agostini, S., Mazzarini, F., Innocenti, F., Manetti, P., Haller, M.J., Lahsen, A.A., 2000. The Pali Aike volcanic field, Patagonia: slab-window magmatism near the tip of South America. Tectonophysics 321, 407–427.

Dunlop, D.J., 2002. Theory and application of the Day plot (Mrs/Ms versus Hcr/Hc) 1.Theoretical curves and tests using titanomagnetite data. J. Geophys. Res. 107 (B3), 1–22.

Dunlop, D.J., Özdemir, Ö., 1997. Rock Magnetism: Fundamentals and Frontiers. Cambridge University Press, Cambridge, New York.

Dunlop, D.J., Özdemir, O., 2007. Magnetizations in rocks and minerals. In: Schubert, G. (Ed.), 2007. Geomagnetism, Treatise on Geophysics, vol. 5. Elsevier, pp. 277–336.

Gebhardt, A.C., Ohlendorf, C., Niessen, F., De Batist, M., Anselmetti, F.S., Ariztegui, D., Kliem, P., Wastegård, S., Zolitschka, B., 2012. Seismic evidence of up to 200 m lake-level change in Southern Patagonia since MIS 4. Sedimentology 59, 1087–1100.

Gogorza, C.S.G., Sinito, A.M., Lirio, J.M., Nuñez, H., Chaparro, M., Vilas, J.F., 2002. Paleosecular variations 0–19,000 years recorded by sediments from Escondido Lake (Argentina). Phys. Earth Planet. Int 133, 35–55.

Gogorza, C.S.G., Lirio, J.M., Nuñez, H., Chaparro, M.A.E., Bertorello, H.R., Sinito, A.M., 2004. Paleointensity studies on Holocene–Pleistocene sediments from lake Escondido, Argentina. Phys. Earth Planet. Int. 145, 219–238.

Gogorza, C.S.G., Irurzun, M.A., Chaparro, M.A.E., Lirio, J.M., Nuñez, H., Bercoff, P.G., Sinito, A.M., 2006. Relative paleointensity of the geomagnetic field over the last 21,000 years BP from sediment cores, Lake El Trébol (Patagonia, Argentina). Earth Planets Space 58, 1323–1332.

Gogorza, C.S.G., Sinito, A.M., Ohlendorf, C., Kastner, S., Zolitschka, B., 2011. Paleosecular variation and paleointensity records for the last millennium from southern South America (Laguna Potrok Aike, Santa Cruz, Argentina). Phys. Earth Planet. Int. 184, 41–50.

Gogorza, C.S.G., Irurzun, M.A., Sinito, A.M., Lisé-Pronovost, A., St-Onge, G., Haberzettl, T., Ohlendorf, C., Kastner, S., Zolitschka, B., 2012. High-resolution paleomagnetic records from Laguna Potrok Aike (Patagonia, Argentina) for the last 16,000 years. Geochem. Geophys. Geosyst 13, 12.

Gubbins, D., Bloxham, J., 1985. Geomagnetic field analysis—III. Magnetic fields on the core-mantle boundary. Geophys. J. R. Astron. Soc. 80, 695–713.

Guyodo, Y., Valet, J.-P., 1996. Relative variations in geomagnetic intensity from sedimentary records: the past 200 thousand years. Earth Planet. Sci. Lett. 143 (1–4), 23–36.

Haberzettl, T., Corbella, H., Fey, M., Janssen, S., Lücke, A., Mayr, C., Ohlendorf, C., Schäbitz, F., Schleser, G.H., Wille, M., Wulf, S., Zolischka, B., 2007. Lateglacial and Holocene wet-dry cycles in southern Patagonia: chronology, sedimentology and geochemistry of a lacustrine record from Laguna Potrok Aike, Argentina. The Holocene 17 (3), 297–310.

Haberzettl, T., Kück, B., Wulf, S., Anselmetti, F., Ariztegui, D., Corbella, H., Fey, M., Janssen, S., Lücke, A., Mayr, C., Ohlendorf, C., Schäbitz, F., Schleser, G.H., Wille, M., Zolitschka, B., 2008. Hydrological variability in southeastern Patagonia and explosive volcanic activity in the southern Andean Cordillera during Oxygen Isotope Stage 3 and the Holocene inferred from lake sediments of Laguna Potrok Aike, Argentina. Palaeogeogr., Palaeoclimatol., Palaeoecol. 259, 213–229.

Haberzettl, T., Anselmetti, F.S., Bowen, S.W., Fey, M., Mayr, C., Zolitschka, B., Ariztegui, D., Mauz, B., Ohlendorf, C., Kastner, S., Lücke, A., Schäbitz, F., Wille, M., 2009. Late Pleistocene dust deposition in the Patagonian steppe – extending and refining the paleoenvironmental and tephrochronological record from Laguna Potrok Aike back to 55 ka. Quat. Sci. Rev. 28, 2927–2939.

Hahn, A., Kliem, P., Ohlendorf, C., Zolitschka, B., Rosen, P., ahe the PASADO science team, 2013. Climate induced changes in the content of carbonaceous and organic matter of sediments from Laguna Potrok Aike (Argentina) during the past 50 ka inferred from infrared spectroscopy. Quat. Sci. Rev. 71, 154–166.

Hartmann, G.A., Pacca, I.G., 2009. Time evolution of the South Atlantic magnetic anomaly. An. Acad. Bras. Ciênc 81 (2), 243–255.

Hayashida, A., Ali, M., Kuniko, Y., Kitagawa, H., Torii, M., Takemura, K., 2007. Environmental magnetic record and paleosecular variation data for the last 40 kyrs from the Lake Biwa sediments, Central Japan. Earth Planets Space 59, 807–814.

Hodgson, D.A., Roberts, S.J., Bentley, M.J., Carmichael, E.L., Smith, J.A., Verleyen, E., Vyverman, W., Geissler, P., Leng, M.J., Sanderson, D.C.W., 2009. Exploring former subglacial Hodgson Lake. Paper II: Palaeolimnology. Quat. Sci. Rev. 28, 2310–2325.

Hounslow, M.W., Maher, B.A., 1999. Laboratory procedures for quantitative extraction and analysis of magnetic minerals from sediments. In: Walden, J., Oldfield, F., Smith, J. (Eds.), Environmental Magnetism, a Practical Guide. Quaternary Research Association, Technical Guide No. 6, pp. 139–164.

Hulot, G., Eymin, C., Langlais, B., Mandea, M., Olson, N., 2002. Small-scale structure of the geodynamo inferred from Ørsted and Magsat satellite data. Nature 416, 620–623.

Irurzun, M.A., Gogorza, C.S.G., Sinito, A.M., Lirio, J.M., Nuñez, H., Chaparro, M.A.E., 2006. Paleosecular variations recorded by sediments from Lake El Trébol, Argentina. Phys. Earth Planet. Int. 154, 1–17.

Kaiser, J., Lamy, F., Hebbeln, D., 2005. A 70-kyr sea surface temperature record off southern Chile (Ocean Drilling Program Site 1233). Paleoceanography 20, PA4009.

King, J.W., Banerjee, S.K., Marvin, J.A., Özdemir, Ö., 1982. A comparison of different magnetic methods for determining the relative grain size of magnetite in natural materials: some results from lake sediments. Earth Planet. Sci. Lett. 59, 404–419.

King, J.W., Benerjee, S.K., Marvin, J., 1983. A new rock-magnetic approach to selecting sediments for geomagnetic paleointensity studies: application to paleointensity for the last 4000 years. J. Geophys. Res. 88 (B7), 5911–5921.

Kirschvink, J.L., 1980. The least-squares line and plane and the analysis of paleomagnetic data. Geophys. J. Roy. Astr. Soc. 62, 699–718.

Kliem, P., Enters, D., Hahn, A., Ohlendorf, C., Lisé-Pronovost, A., St-Onge, G., Wastegård, S., Zolitschka, B., and the PASADO science team, 2013. Lithology, radiocarbon dating and sedimentological interpretation of the 51 ka BP lacustrine record from Laguna Potrok Aike, Southern Patagonia. Quat. Sci. Rev. 71, 54–69.

Knudsen, M.F., Riisager, P., Donadini, F., Snowball, I., Muscheler, R., Korhonen, K., Pesonen, L.J., 2008. Variations in the geomagnetic dipole moment during the Holocene and the past 50 kyr. Earth Planet. Sci. Lett. 272 (1–2), 319–329.

Korte, M., Constable, C., 2011. Improving geomagnetic field reconstructions for 0–3 ka. Phys. Earth Planet. Int. 188 (3–4), 247–259.

Korte, M., Genevey, A., Constable, C.G., Frank, U., Schnepp, E., 2005. Continuous geomagnetic field models for the past 7 millennia: 1. A new global data compilation. Geochem. Geophys. Geosyst. 6, Q02H15.

Korte, M., Constable, C., Donadini, F., Holme, R., 2011. Reconstructing the Holocene geomagnetic field. Earth Planet. Sci. Lett. 312, 497–505.

Laj, C., Channell, J.E.T., 2007. Geomagnetic excursions. In: Kono, M. (Ed.), Treatise on Geophysics. Geomagnetism, vol. 5. Elsevier, Amsterdam, pp. 373–416.

Laj, C., Kissel, C., Scao, V., Beer, J., Muscheler, R., Wagner, G., 2002. Geomagnetic intensity variations at Hawaii for the past 98 kyr from core SOH4 (Big Island): new results. Phys. Earth Planet. Int. 129, 205–243.

Laj, C., Kissel, C., Beer, J., 2004. High resolution global paleointensity stack since 75 kyrs (GLOPIS-75) calibrated to absolute values. In: Channell, J.E.T., Kent, D.V., Lowrie, W., Meert, J.G. (Eds.), Timescales of the Paleomagnetic Field. AGU Geophysical Monograph, vol. 145.

Levi, S., Banerjee, S.K., 1976. On the possibility of obtaining relative paleointensities from lake sediments. Earth Planet. Sci. Lett. 29, 219–226.

Lisé-Pronovost, A., St-Onge, G., Brachfeld, S., Barletta, F., Darby, D., 2009. Paleomagnetic constraints on the Holocene stratigraphy of the Arctic Alaskan margin. Global Planet. Change 68, 85–99.

Lund, S.P., Stoner, J.S., Channell, J.E.T., Acton, G., 2006a. A summary of Bruhnes paleomagnetic field variability recorded in Ocean Drilling Program cores. Phys. Earth Planet. Int. 156 (3–4), 194–204.

Lund, S.P., Stoner, J., Lamy, F., 2006b. Late Quaternary paleomagnetic secular variation and chronostratigraphy from ODP sites 1233 and 1234. In: Tiedemann, R., Mix, A.C., Richter, C., Ruddiman, W.F. (Eds.), 2006b. Proceedings of the Ocean Drilling Program, Scientific Results, vol. 202.

Macrì, P., Sagnotti, L., Dinares-Turell, J., Caburlotto, A., 2005. A composite record of Late Pleistocene relative geomagnetic paleointensity from the Wilkes Land Basin (Antarctica). Phys. Earth Planet. Int. 151, 223–242.

Macrì, P., Sagnotti, L., Dinarès-Turell, J., Caburlotto, A., 2010. Relative geomagnetic paleointensity of the Brunhes Chron and the Matuyama–Brunhes precursor as recorded in sediment core from Wilkes Land Basin (Antarctica). Phys. Earth Planet. Int. 179, 72–86.

Mayr, C., Wille, M., Haberzettl, T., Fey, M., Janssen, S., Lücke, A., Ohlendorf, C., Oliva, G., Schäbitz, F., Schleser, G.H., Zolitschka, B., 2007. Holocene variability of the Southern Hemisphere westerlies in Argentinean Patagonia (52°S). Quat. Sci. Rev. 26, 579–584.

Mazaud, A., 2005. User-friendly software for vector analysis of the magnetisation of long sediment cores. Geochem. Geophys. Geosyst. 6, 1–5.

Mazaud, A., Sicre, M.A., Ezat, U., Pichon, J.J., Duprat, J., Laj, C., Kissel, C., Beaufort, L., Michel, E., Turon, J.L., 2002. Geomagnetic-assisted stratigraphy and sea surface temperature changes in core MD94-103 (Southern Indian Ocean): possible implications for North–South climatic relationships around H4. Earth Planet. Sci. Lett. 201 (1), 15, pp. 159–170.

Merrill, R.T., McFadden, P.L., 1994. Geomagnetic field stability; reversal events and excursions. Earth Planet. Sci. Lett. 121, 57–69.

Muscheler, R., Beer, J., Kubik, P.W., Synal, H.-A., 2005. Geomagnetic field intensity during the last 60,000 years based on ^{10}Be and ^{36}Cl from the Summit ice cores and ^{14}C. Quat. Sci. Rev. 24, 1849–1860.

Nilsson, A., Muscheler, R., Snowball, I., Aldahan, A., Possnert, G., Augustinus, P., Atkin, D., Stephens, T., 2011. Multi-proxy identification of the Laschamp geomagnetic field excursion in Lake Pupuke, New Zealand. Earth Planet. Sci. Lett. 311 (1–2), 155–164.

Nowaczyk, N.R., Knies, J., 2000. Magnetostratigraphic results from the eastern Arctic Ocean: AMS ^{14}C ages and relative palaeointensity data of the Mono Lake and Laschamp geomagnetic reversal excursions. Geophys. J. Int. 140 (1), 185–197.

Nowaczyk, N.R., Antonow, M., Knies, J., Spielhagen, R.F., 2003. Further rock magnetic and chronostratigraphic results on reversal excursions during the last 50 ka as derived from northern high latitudes and discrepancies in precise AMS ^{14}C dating. Geophys. J. Int. 155 (5), 1065–1080.

Opdyke, N.D., Channell, J.E.T., 1996. Magnetic Stratigraphy. Academic Press, San Diego, CA.

Paillard, D., Labeyrie, L., Yiou, P., 1996. Macintosh program performs time-series analysis. Eos Trans. AGU 77, 379.

Peck, J.A., King, J.W., Colman, S.M., Kravchinsky, V.A., 1996. An 84-kyr paleomagnetic record from the sediments of Lake Baikal Siberia. J. Geophys. Res. 101 (B5), 11365–11385.

Recasens, C., Ariztegui, D., Gebhardt, C., Gogorza, C., Haberzettl, T., Hahn, A., Kliem, P., Lisé-Pronovost, A., Lücke, A., Maidana, N.I., Mayr, C., Ohlendorf, C., Schäbitz, F., St-Onge, G., Wille, M., Zolitschka, B, and the PASADO Science Team, 2011. New insights into paleoenvironmental changes in Laguna Potrok Aike, Southern Patagonia, since the Late Pleistocene: the PASADO multiproxy record. The Holocene. doi:10.1177/0959683611429833.

Roberts, A.P., 2008. Geomagnetic excursions: knowns and unknowns. Geophys. Res. Lett. 35, L17307.

Roberts, A.P., Winklhofer, M., 2004. Why are geomagnetic excursions not always recorded in sediments? Constraints from post-depositional remanent magnetisation lock-in modelling. Earth Planet. Sci. Lett. 227 (3–4), 345–359.

Ross, P.-S., Delpit, S., Haller, M.J., Németh, K., et Corbella, H., 2011. Influence of the substrate on maar-diatreme volcanoes – an example of a mixed setting from the Pali Aike volcanic field, Argentina. J. Volcanol. Geoth. Res. 201 (1), 253–272.

Schaefer, J.M., Denton, G.H., Barrell, D.J.A., Ivy-Ochs, S., Kubik, P.W., Andersen, B.G., Phillips, F.M., Lowell, T.V., Schluchter, C., 2006. Near-synchronous interhemispheric termination of the last glacial maximum in mid-latitudes. Science 312, 1510–1513.

Schneider, D.A., Mello, G.A., 1996. A high-resolution marine sedimentary record of geomagnetic intensity during the Brunhes Chron. Earth Planet. Sci. Lett. 144 (1–2), 297–314.

Singer, B.S., 2007. Polarity transitions: radioisotopic dating. In: Bervera, E.H., Gubbins, D. (Eds.), Encyclopedia of Geomagnetism and Paleomagnetism. Springer-Verlag, pp. 834–839.

Singer, B.S., Guillou, H., Jicha, B.R., Laj, C., Kissel, C., Beard, B.L., Johnson, C.M., 2009. $^{40}Ar/^{39}Ar$, K–Ar and $^{230}Th–^{238}U$ dating of the Laschamp excursion: a radioisotopic tie-point for ice core and climate chronologies. Earth Planet. Sci. Lett. 286 (1–2), 80–88.

Snowball, I., Sandgren, P., 2004. Geomagnetic field intensity changes in Sweden between 9000 and 450 cal BP: extending the record of "archeomagnetic jerks" by means of lake sediments and the pseudo-Thellier technique. Earth Planet. Sci. Lett. 227, 361–376.

St-Onge, G., Stoner, J.S., Hillaire-Marcel, C., 2003. Holocene paleomagnetic records fromthe St. Lawrence Estuary, eastern Canada: centennial- to millennial-scale geomagnetic modulation of cosmogenic isotopes. Earth Planet. Sci. Lett. 209, 113–130.

Stoner, S.J., St-Onge, G., 2007. Magnetic stratigraphy in paleooceanography: reversal, excursion, paleointensity and secular variation. In: Hillaire-Marcel, C., de Vernal, A. (Eds.), Proxies in Late Cenozoic Paleoceanography. Elsevier, pp. 99–138.

Stoner, J.S., Laj, C., Channell, J.E.T., Kissel, C., 2002. South Atlantic and North Atlantic geomagnetic paleointensity stacks (0–80 ka): implications for inter-hemispheric correlation. Quat. Sci. Rev. 21, 1141–1151.

Stoner, J.S., Channell, J.E.T., Hodell, D.A., Charles, C.D., 2003. A 580 kyr paleomagnetic record from the sub-Antarctic South Atlantic (Ocean Drilling Program Site 1089). J. Geophys. Res. 108 (B5), 2244.

Stoner, J.S., Jennings, A., Kristjánsdóttir, G.B., Dunhill, G., Andrews, J.T., Hardardóttir, J., 2007. A paleomagnetic approach toward refining Holocene radiocarbon-based chronologies: paleoceanographic records from the north Iceland (MD99-2269) and east Greenland (MD99-2322) margins. Paleoceanography 22, PA1209.

Sugden, D.A., McCulloch, R.D., Bory, A.J.-M., Hein, A.S., 2009. Influence of Patagonian glaciers on Antarctic dust deposition during the last glacial period. Nature geosciences 2, 281–285.

Tauxe, L., 1993. Sedimentary records of relative paleointensity of the geomagnetic field: theory and practice. Rev. Geophys. 31 (3), 319–354.

Tauxe, L., 2005. Inclination flattening and the geocentric axial dipole hypothesis. Earth Planet. Sci. Lett. 233 (3–4), 247–261.

Tauxe, L., Wu, G., 1990. Normalized remanence in sediments of the Western Equatorial Pacific: relative paleointensity of the geomagnetic field? J. Geophys. Res. 95 (B8), 12337–12350.

Tauxe, L., Pick, T., Kok, Y.S., 1995. Relative paleointensity in sediments: a pseudo-Thellier approach. Geophys. Res. Lett. 22, 2885–2888.

Tauxe, L., Mullender, T.A.T., Pick, T., 1996. Potbellies, wasp-waists, and superparamagnetism in magnetic hysteresis. J. Geophys. Res. 101 (B1), 571–583.

Teanby, N., Laj, C., Gubbins, D., Pringle, M., 2002. A detailed palaeointensity and inclination record from drill core SOH1 on Hawaii. Phys. Earth Planet. Int. 131, 101–140.

Wagner, G., Beer, J., Laj, C., Kissel, C., Masarik, J., Muscheler, R., Synal, H.-A., 2000. Chlorine-36 evidence for the Mono Lake event in the summit GRIP ice core. Earth Planet. Sci. Lett. 181, 1–6.

Weeks, R., Laj, C., Endigoux, L., Fuller, M., Roberts, A., Manganne, R., Blanchard, E., Goree, W., 1993. Improvements in long-core measurements techniques: applications in paleomagnetism and paleoceanography. Geophys. J. Int. 114, 651–662.

Willmott, V., Domack, E.W., Canals, M., Brachfeld, S., 2006. A high resolution paleointensity record from the Gerlache-Boyd paloe-ice stream region, northern Antarctic Peninsula. Quat. Res. 66, 1–11.

Xuan, C., Channell, J.E.T., 2009. UPmag: MATLAB software for viewing and processing u-channel or other pass-through paleomagnetic data. Geochem. Geophys. Geosyst. 10, Q10Y07.

Xuan, C., Channell, J.E.T., 2010. Origin of apparent magnetic excursions in deep-sea sediments from Mendeleev-Alpha Ridge, Arctic Ocean. Geochem. Geophys. Geosyst. 11, Q02003.

Zhu, J., Lücke, A., Wissel, H., Mayr, C., Ohlendorf, C., Zolitschka, B., The PASADO Science Team, 2013. Environmental instability at the last Glacial–Interglacial transition in Patagonia Argentina the stable isotope record of bulk sedimentary organic matter from Laguna Potrok Aike. Quat. Sci. Rev. 71, 205–218.

Zolitschka, B., Schäbitz, F., Lücke, A., Corbella, H., Ercolano, B., Fey, M., Haberzettl, T., Janssen, S., Maidana, N., Mayr, C., Ohlendorf, C., Oliva, G., Paez, M.M., Schleser, G.H., Soto, J., Tiberi, P., Wille, M., 2006. Crater lakes of the Pali Aike volcanic field as key sites for paleoclimatic and paleocological reconstructions in southern Patagonia, Argentina. J. South Am. Earth Sci. 21, 294–309.

Zolitschka, B., Anselmetti, F., Ariztegui, D., Corbella, H., Francus, P., Ohlendorf, C., Schäbitz, F., the PASADO Scientific Drilling team, 2009. The Laguna Potrok Aike Scientific Drilling Project PASADO (ICDP Expedition 5022). Scientific Drilling 8, 29–34.